Published in final edited form as:
Toxicol Pathol. 2013 July ; 41(5): 744–760. doi:10.1177/0192623312464308.

Anchoring Hepatic Gene Expression with Development of Fibrosis and Neoplasia in a Toxicant-Induced Fish Model of Liver Injury

Arnaud J. Van Wettere[1,2], **J. Mac Law**[1,2], **David E. Hinton**[3], and **Seth W. Kullman**[2,4]

[1]Department of Population Health and Pathobiology, College of Veterinary Medicine, North Carolina State University, Raleigh, North Carolina, USA

[2]Center for Comparative Medicine and Translational Research, College of Veterinary Medicine, North Carolina State University, Raleigh, North Carolina, USA

[3]Nicholas School of the Environment, Duke University, Durham, North Carolina, USA

[4]Department of Environmental and Molecular Toxicology, North Carolina State University, Raleigh, North Carolina, USA

Abstract

Fish have been used as laboratory models to study hepatic development and carcinogenesis but not for pathogenesis of hepatic fibrosis. In this study, a dimethylnitrosamine-induced fish model of hepatic injury was developed in Japanese medaka (*Oryzias latipes*) and gene expression was anchored with the development of hepatic fibrosis and neoplasia. Exposed livers exhibited mild hepatocellular degenerative changes 2 weeks post-exposure. Within six weeks hepatic fibrosis/cirrhosis was evident with development of neoplasia by 10 weeks. Stellate cell activation and development of fibrosis was associated with upregulation of tgfb1,tgfb receptor 2, smad3a, smad3b, ctnnb1, myc, mmp2, mmp14a, mmp14b, timp2a, timp2b, timp3, col1a1a, and col1a1b, and a less pronounced increase in *mmp13* and *col4a1*expression. *Tgfb receptor I* expression was unchanged. Immunohistochemistry suggested that biliary epithelial cells and stellate cells were the main producers of TGF-β1. This study identified a group of candidate genes likely to be involved in the development of hepatic fibrosis, and demonstrated that the TGF-β pathway likely plays a major role in the pathogenesis. These results support the medaka as a viable fish model of hepatic fibrosis.

Keywords

dimethylnitrosamine; liver; fibrosis; neoplasia; medaka; *Oryzias latipes*; gene expression

Arnaud J. Van Wettere, Department of Population Health and Pathobiology, College of Veterinary Medicine, North Carolina State University, 1060 William Moore Drive, Raleigh, NC 27607, USA; Phone: ++ 1 919 515 7410; arnaud_vanwettere@ncsu.edu.

INTRODUCTION

Small fish models such as the zebrafish (*Danio rerio*) and the medaka (*Oryzias latipes)* have been used increasingly in the last 4 decades to study genetic regulation of development, carcinogenesis, high-throughput screening of chemicals, and environmental monitoring (Hinton et al., 2009). In order to accurately extrapolate findings obtained from aquatic models to humans, it is critical to understand the differences and similarities in organ structure, response to injury and molecular mechanisms between these phylogenetically distant species. Given its fundamental function in metabolizing chemicals, the liver is an important target organ of toxicity and has received considerable attention. However the information available regarding the hepatic cellular response to injury in small fish models and the relevant molecular mechanism(s) remain limited (Wolf and Wolfe, 2005).

In mammals, irrespective of the cause, chronic liver injury results in hepatic fibrosis, the end-stage of which is called cirrhosis, and is associated with chronic liver functional impairment. In the United States, chronic liver disease was the 12th leading cause of death in 2006 (Heron et al., 2009). Abusive alcohol consumption, hepatotoxins (e.g. Aflatoxin B1), autoimmunity, nonalcoholic fatty liver disease and infections with Hepatitis B and Hepatitis C-viruses are the main cause of chronic hepatitis (Sherman, 2010). Liver cancer can be the ultimate consequence of chronic liver injury (Wallace et al., 2008). Hepatocellular carcinoma (HCC) alone is the fifth most common cancer and the third cause of cancer-related death world-wide (Parkin et al., 2001; Wallace et al., 2008). Given the very limited therapeutic options, understanding the intricate cellular interactions implicated in liver fibrogenesis and subsequent progression to neoplasia is crucial.

Major events in the development of hepatic fibrosis in mammals involve activation of the TGF-β pathway and hepatic stellate cells (HSC) that result in an increased production of collagen, altered balance between metalloproteinases (MMP) and tissue inhibitors of metalloproteinases (TIMP) and, as an end result, excessive deposition of collagenous extracellular matrix in the hepatic parenchyma (Hernandez-Gea and Friedman, 2010).

Dimethynitrosamine (DMN) is a potent carcinogenic hepatotoxin previously used in rodents to model human hepatic fibrosis, cirrhosis and HCC (Ala-Kokko et al., 1987; Jezequel et al., 1987; George et al., 2001; Tada et al., 2001; Hyon et al., 2011). In a comparative model, Hobbie et al. (2011) reported that Japanese medaka fish (*Oryzias latipes*) exposed to DMN developed morphological hepatic changes similar to those observed in human fibrotic livers and the well-established DMN-induced rat model of hepatic fibrosis (Ala-Kokko et al., 1987; Jezequel et al., 1987; Ohara et al., 2007; Hobbie et al., 2011; Hyon et al., 2011). Currently, knowledge of the mechanisms of hepatic fibrosis and progression to neoplasia in fish is limited. Using immunohistochemical approaches, Hobbie et al. (2011) demonstrated increased muscle specific actin (MSA), TGF-β1 and SMAD 3 labeled cells in livers of DMN exposed medaka. These results suggested that myofibroblastic transdifferentiation of HSCs, and up-regulation of the TGF- β pathways occur in medaka liver fibrosis similar to that observed in rodent models and humans (Hobbie et al., 2011).

In this study we refined the DMN-exposure parameters to reliably induce severe hepatic fibrosis/cirrhosis and hypothesized that activation of hepatic stellate cells and upregulation of the canonical TGF-β pathways, MMPs and TIMPs genes are critical steps in the development of hepatic fibrosis after DMN-induced hepatic injury in Japanese medaka. The expression of key genes involved in the pathogenesis of fibrosis in mammals was anchored to the activation of medaka hepatic stellate cells and deposition of collagenous matrix. Our overarching aim using the medaka fish model, was to enhance our knowledge of the comparative vertebrate pathogenesis of hepatic fibrosis.

MATERIALS and METHODS

Chemicals

Dimethylnitrosamine (DMN, C2H6N2O; 99.9%, CAS 62-75-9, MW 74.08 g/mol) was obtained from Sigma-Aldrich (St. Louis, MO). The air tight brown bottle of DMN was stored within a metal container at 4°C. All chemicals and reagents used in this study were of the highest purity available from commercial resources.

Medaka and DMN Exposures

Male and female orange-red Japanese medaka were obtained initially as three-month-old fish from an in-house stock population maintained under recirculating freshwater aquaculture conditions at the Department of Molecular and Environmental Toxicology, North Carolina State University (NCSU), Raleigh, NC. Fish were acclimated in 10 gallon aquarium tanks filled with reconstituted (0.5 g/liter Instant Ocean® salts, Aquarium System Inc. Mentor, OH) reverse osmosis–purified (RO) water within a recirculating, freshwater culture system. The system was maintained under an artificial light photoperiod (16 hours light/8 hours dark) with water temperature of 26 ± 0.5°C, pH of ~ 6.5 and conductivity of 600 to 800 μS. Dry food (Otohime B1, Reed Mariculture, Campbell, CA) was fed 4 times per day through automated feeders. Animal care and use were in conformity with protocols approved by the NCSU Institutional Animal Care and Use Committee in accordance with the National Academy of Sciences Guide for the Care and Use of Laboratory Animals.

When the fish were 6-8 months old, one hundred and seventy medaka (male and female) were exposed to 100 μg/L (ppm) DMN for 2 weeks in the ambient water. Ninety medaka (male and female) were used as unexposed controls. Fish were exposed in 4-liter glass beakers containing 3 liters of reconstituted RO water as described above. For all exposures, medaka were randomly distributed among the 4-liter glass beakers, 10–12 fish per beaker. The beakers were placed within a recirculating, heated water bath to maintain temperature at 26 ± 0.5°C throughout the exposures. DMN dilutions were made from the DMN stock solution (in H_2O) and prepared new prior to each exposure. DMN spiked water (95% water change) was replaced every 3 days to compensate for photodegradation of the compound and maintain water quality (Hobbie et al., 2011). Ammonia levels remained under 0.25 mg/liter throughout the entire study. During the exposure, fish were fed once daily with dry fish food (Otohime B1) and observed twice daily for behavioral responses and/or signs of overt toxicity. Following exposure, fish were removed from the exposure beakers, gently rinsed in

RO water, and replaced in 10 gallon aquarium tanks for up to 12 weeks at a density of 40 fish per tank).

Sampling Method and Tissue Processing

Twenty four exposed and 14 control fish were euthanatized with an overdose of tricaine methanesulfonate (300 mg/liter; MS-222, Argent Laboratories, Redmond, WA) at 2, 4, 6, or 10 weeks post exposure. The gender of the fish was determined by examining external sex characteristics and gonadal phenotype. The liver of 20 exposed and 10 control fish were examined grossly, harvested and cut into two approximately equal-sized pieces. One was snap frozen in liquid nitrogen for RNA isolation and quantitative PCR (qPCR) analysis. The other piece was fixed in freshly made 4% paraformaldehyde solution (pH 7.2) for 24 hours, and transferred to 70% ethanol for histopathology. A few small samples (1 × 1 mm) of 4 exposed and control livers were fixed in 4% formaldehyde and 1% glutaraldehyde buffered in monobasic sodium phosphate, pH 7.2-7.4 (4F:1G) for transmission electron microscopy (McDowell and Trump, 1976). To detect infectious diseases or background lesions in organs other than the liver that could have influenced the study results, a subset of fish was examined whole by histology. The celomic cavities of four control and four exposed fish were incised along the ventral midline to enhance fixative penetration and fish were fixed as above for 24 hours, demineralized in 10% formic acid for 24 hours, and transferred to 70% ethanol for histopathology.

Histology

Paraformaldehyde –fixed livers were processed, and embedded in paraffin according to routine histologic techniques. Sections, 5-μm thick, were stained with hematoxylin and eosin (H&E) and examined by light microscopy. Sections of liver were also stained with Masson's trichrome stain according to standard methods. Medaka liver lesions were identified based on criteria set by a consensus of the US National Toxicology Program pathology working group and the International Harmonization of Nomenclature and Diagnostic Criteria for Lesions in Rats and Mice (INHAND) project (Boorman et al., 1997; Thoolen et al., 2010).

Immunohistochemistry

Immunohistochemical studies were performed using single and double staining techniques. Five-micrometer thick paraffin sections from all livers were used for MSA and pancytokeratin (CK) immunohistochemistry. The MSA primary antibody used was a mouse monoclonal antibody that recognizes a 42-kD protein specific for actin in skeletal, cardiac, and smooth muscle (BioGenex Laboratories, San Ramon, CA. Catalogue # MU090-UC). The CK AE1/AE3 antibody used was a cocktail of 2 mouse monoclonal antibodies that recognize several acidic (10, 14 to 16, 19), and all basic (1- 8) human cytokeratins (BioGenex Laboratories, San Ramon, CA. Catalogue # AM0751-5M). The TGF-β1 antibody was a rabbit polyclonal antibody that recognizes the human TGF-β1 C-terminus (Santa Cruz Biotechnology Inc., Santa Cruz, CA. Catalogue # sc 146). Tissue sections were deparaffinized in xylene, rehydrated in a graded series of ethanol and rinsed in distilled water. Antigen retrieval was performed only for CK staining by heating the slides at 99°C in a 10 mM sodium citrate solution at pH 6 for 10 minutes in a vegetable steamer (Oster 5712 food steamer, Maitland, FL). Following antigen retrieval a cool down period of 10 minutes

in the warm sodium citrate buffer preceded rinsing of the slides in 1X phosphate-buffered saline (PBS). Slides were treated with 3% hydrogen peroxide for 10 minutes to block activity of endogenous peroxidases. Goat serum was applied for 20 minutes to prevent nonspecific binding of the secondary antibody (BioGenex San Ramon, CA).

For single staining, avidin and biotin blocks were applied successively for 15 minutes each (BioGenex San Ramon, CA). Tissues were incubated with the MSA antibody (1/100 dilution) or CK antibody (sold prediluted) for 30 minutes at room temperature, or with the TGF-β1 antibody (1/500) overnight at 4°C. For double staining, tissues were incubated with a primary antibody cocktail of MSA and TGF-β1 or CK and TGF-β1 antibodies overnight at 4°C. The slides were rinsed in 1X PBS. For single staining, the slides were incubated with the secondary antibody for 20 minutes (BioGenex San Ramon, CA). After a wash in 1X PBS, tissue sections were then treated for 20 minutes with streptavidin peroxidase (BioGenex San Ramon, CA). For double staining the slides were incubated with a polymer cocktail detection system for 30 minutes at room temperature (anti-mouse/horseradish peroxidase (HRP) + anti-rabbit/alkaline phosphatase (AP), MultiVisionPolymer Detection System, Thermo Fisher Scientific, Lab Vision Corporation, Fremont, CA). Following a final wash in 1X PBS, development was achieved by treatment of tissue with liquid 3,3-diaminobenzidine (DAB) chromogen for 15 second to 1 minutes (Vector Lab, Burlingame, CA). For double staining, development was achieved using first LVBlue (Thermo Fisher Scientific, Lab Vision Corporation, Fremont, CA) for AP activity followed by DAB for HRP activity. After a wash in tap water, the slides with single staining were counterstained with Mayer's hematoxylin for 20–40 seconds and cover slipped. The slides with double staining were counterstained lightly with methyl green and cover slipped. For each immunohistochemical reaction, appropriate controls were run. The primary antibody was omitted and replaced by non-immune serum of the same animal source in the negative control. Sections of normal intestine and liver were included on each slide to serve as positive controls.

Morphometry

The number of activated stellate cells was determined by measuring the percentage area occupied by MSA immunoreactivity. For each liver histologic section, 15 randomly selected sites were photographed at 600X using an Olympus DP 25 digital microscope camera with the CellSens® digital imaging software mounted on an Olympus BH 51 microscope (Olympus Corporation, Tokyo, Japan). The images were manually thresholded to highlight the MSA immunoreactive cells and background was subtracted using Adobe Photoshop CS4 (PhotoshopCS4; Adobe Systems, Park Avenue, San Jose, CA, USA). The same setting was used for all images in a given data set. The best setting for background subtraction was determined empirically by testing images with the lowest and highest amount of MSA immunopositivity. Finally, the area fraction covered with the MSA positive cells, expressed as a percentage of the picture surface area, was measured using an automatic image analysis system (ImageJ, NIH, Bethesda, MD).

The extent of liver fibrosis was determined semi-quantitatively and assigned a 0 to 3 score using Masson's trichrome stained slides. The scale used was as follows: 0: no fibrosis; 1,

mild fibrosis (small amount of fibrous tissue dissecting between the hepatocyte tubules); 2, moderate fibrosis (moderate amount of fibrous tissue dissecting between hepatocyte tubules with occasional presence of hepatocellular nodules; and, 3, severe fibrosis/cirrhosis (frequent large fibrous tissue septa dissecting and isolating variably sized aggregates of hepatocytes, and frequent hepatocellular nodules).

Electron Microscopy

For transmission electron microscopy (TEM) liver samples fixed in 4F:1G were dehydrated in a graded series of ethanol, and embedded in Spurr resin (Dykstra, 1993). To determine whether structures of interest were in planar sections of the block face, semithin sections, 0.5 μm thick, stained with 1% toluidine blue in 1% sodium borate, were examined under a light microscope. Ultrathin sections, 90 nm thick, of appropriate blocks were stained with uranyl acetate and lead citrate and examined with a FEI/Philips EM 208S transmission electron microscope (Laboratory for Advanced Electron and Light Optical Methods, NCSU, Raleigh, NC).

Reverse transcription and real-time PCR

Liver samples were homogenized using the Bullet Blender (Next Advance, Averill Park, NY) with 0.5 mm zirconium oxide beads (setting 6 for 3 minutes) and total RNA was extracted using RNA Bee (Tel-Test Inc., Friendswood, TX) according to the manufacturer's instructions. RNA purity (260/280 ratio) and quantity were determined using a NanoDrop ND-1000 spectrophotometer (NanoDrop Technologies, Wilmington, DE). RNA quality was determined using RNA Nano chips with an Agilent Bioanalyzer 2100 (Agilent Technologies, Palo Alto, CA). Only RNA samples with RNA integrity number > 7 and a 260/280 ration between 1.75 and 2.05 were used for qPCR analysis and these were stored at −80°C to minimize degradation. RNA was reverse transcribed into cDNA using 1 μg total RNA and the high-capacity cDNA master kit from Applied Biosystems (Foster City, CA) as per the manufacturer's instructions with random hexamer as primer and processed using quantitative, real-time PCR (qPCR).

Selected genes were identified in the medaka genome (http://www.ensembl.org/Oryzias_latipes/Info/Index) and assigned gene names consistent withthe zebrafish nomenclature guidelines (https://wiki.zfin.org/display/general/ZFIN+Zebrafish+Nomenclature+Guidelines). All duplicated genes were described as "a" and "b" based on the orthology with zebrafish genes. Specific primers were designed for: tgfb1, tgfbr1, tgfbr2, smad3a, smad3b, ctnnb1, myc, mmp2, mmp13, mmp14a, mmp14b, timp2a, timp2b, timp3, col1a1a, col1a1b, and *col4a1* (Table 1). The efficiency of each primer was tested to fall between 90 and 110%.

cDNAs were PCR amplified separately in triplicate using a 96-well PCR plate and an ABI PRISM 7000 Sequence Detection System (Applied Biosystems, Foster City, CA). Relative levels of the gene transcripts of interest listed above were measured using qPCR and normalized to ribosomal protein L7 (RPL-7) (Zhang and Hu, 2007). Each 25 μl real-time PCR reaction consisted of 2.5 μl (1 ng/μl) first-strand cDNA, 8 μl RNase-free water, 1 μl of 10μM forward primer, 1 μl of 10μM reverse primer, and 12.5 μl of SYBR® Green PCR

Master Mix (AB applied biosystems). Real-time PCR reaction conditions were 50° for 2 minutes, 95°C for 10 minutes followed by 41 cycles of 95°C for 15 s, 60°C for 1 minute, and a last cycle at 95°C for 15 s and 60°C for 15 s. Relative quantitation of gene expression within each reaction was calculated following the method of Livak and Schittgen (2001).

Data analysis and statistics

Liver phenotypes, MSA area data, and fibrosis score were compiled in spreadsheets, and organized by fish case number using Microsoft Excel software (Microsoft; Redmond, WA). The fish were grouped by phenotypes and the MSA percentage area and fibrosis score were calculated for each phenotype and expressed as mean ± SEM. All qPCR data were expressed as the mean mRNA level ± SEM. The difference in gene expression levels or MSA positive areas between the phenotypes was determined using the Mann–Whitney *U* test. The difference in fibrosis scores between phenotypes was determined using Fisher's exact test. A P value less than .05 was considered significant. Correlation between MSA percentage area and fibrosis score or gene expression and fibrosis score was determined using the Spearman rank correlation test. The Fisher's exact test was performed using SAS Version 9.1.3 for Windows (SAS institute, Cary, NC). The Mann–Whitney *U* tests and Spearman rank correlation tests were performed using Sigma Stat 3.0 (SPSS Inc., Chicago, IL, USA).

RESULTS

Among the 170 fish exposed to DMN, 22 (12.9%) died or were euthanized for humane reasons during the grow out period. Given that autolysis occurs rapidly in tank water maintained at 26°C, 14 fish were moderately to severely autolysed at the time they were found and were discarded. The remaining 8 fish were evaluated by histology and had severe hepatic fibrosis/cirrhosis. None of the control fish died or were euthanized on ethical grounds during the duration of the study. For quality control, four additional unexposed and four exposed fish at each time point were processed for whole animal histology and evaluated for undetected infectious disease or background lesion in organs other than the liver that could influence the study results. Based on analysis of whole body parasagittal sections, no evidence of extrahepatic disease or remarkable morphological change was observed in any of the animals examined. Rather, significant morphological changes were limited to livers of exposed fish.

Gross findings

Among the exposed fish, no macroscopic lesions were noted in the fish with hepatocellular degeneration or bile preductular epithelial cell (BPDEC) hyperplasia, although some of the livers were subjectively paler than the majority of the control livers. Livers of fish with hepatic fibrosis had a mildly to markedly bosselated surface and their overall size was subjectively within normal limits or rarely was reduced (Fig.1a). Among the 32 livers diagnosed with hepatic neoplasia on histology, 15 livers had a grossly visible discrete hepatic tumor. The overall liver size was markedly increased and filled most of the celomic cavity in 2 fish.

Histology

Ninety-five half livers from the exposed fish and 56 half livers of control fish were evaluated by histology. Morphological changes and categorization of the livers were performed using H&E and Masson's trichrome-stained liver sections. The control fish showed normal hepatic architecture with the exception of 2 fish collected at 10 weeks post-exposure that had multifocal aggregates of macrophages within the hepatic parenchyma. A Ziehl-Neelsen stain did not reveal any acid-fast bacteria. The cause of the macrophage aggregates in these 2 fish was not determined. They were treated as outliers for the remainder of the study.

Histologic lesions observed in the liver of exposed fish included hepatocellular vacuolar degeneration, Mallory body-like inclusion, hepatocyte hypertrophy, karyomegaly, altered foci, necrosis, collapse of the hepatic architecture, histiocytic inflammation, BPDEC hyperplasia (presumed fish liver bipotential progenitor cell), HSCs hyperplasia, biliary hyperplasia, fibrosis, hepatocellular regeneration, and multinodular reorganization of the liver architecture. Neoplasms included: cholangiocarcinoma (CC), HCC, combined hepatocellular-cholangiocarcinoma (CHC) and a single spindle cell neoplasm, the so-called hemangiopericytoma of fish. A summary of the histologic lesions is presented in Table 2.

The morphological changes in the liver were classified in 5 different phenotypes: 0) normal liver, 1) hepatocellular degeneration, 2) BPDEC hyperplasia, 3) hepatic fibrosis and 4) hepatic fibrosis and neoplasia. A normal liver phenotype was defined as a liver with a normal architecture and an absence to moderate amount of hepatocellular vacuolization (Fig. 1b) (Hardman et al., 2007). The hepatocellular degeneration phenotype was characterized by an increase in hepatocellular vacuolization, presence of globular eosinophilic intra-cytoplasmic inclusions and scattered apoptotic hepatocytes (Fig. 1c). The BPDEC hyperplasia phenotype was characterized by proliferation of small elongated cells with hyperchromatic round to elongated nuclei that separated the hepatocyte tubules and sometimes surrounded individual hepatocytes (Fig. 1d). The BPDEC hyperplasia phenotype closely resembled oval cell hyperplasia that is observed in rodents (Thoolen et al., 2010). The hepatocytes were often variably sized, hypereosinophilic and with reduced amounts of glycogen. The hepatic fibrosis phenotype was characterized by increased fibrous connective tissue separating hepatocyte tubules. In advanced fibrosis stages, the collagenous stroma separated and individualized single or small groups of hepatocytes and hepatocyte tubules (fig. 1e). The hepatic fibrosis with neoplasia phenotype was defined as a fibrotic liver with the presence of a hepatic neoplasm (hepatocellular carcinoma or cholangiocellular carcinoma) (Fig. 1f).

Within exposed groups there were 41 (43%) males, 54 (56%) females and 1 (1%) medaka of undetermined gender. In the control group, we identified 31 (55%) males and 25 (45%) females. Four fish (4%) in the exposed group had no hepatic lesions (Phenotype 0); 22 (23%) had evidence of degenerative hepatocellular changes (phenotype 1); 19 (20%) had marked BPDEC hyperplasia (phenotype 2); 34 (36%) had hepatic fibrosis (phenotype 3); and 16 (17%) developed liver neoplasia (phenotype 4). Among the livers with hepatic neoplasms, 10 fish (63%) were identified with HCC (2 males and 8 females), 3 (19%) with CC (1 males and 2 females), 2 (12%) fish with HCC and a CC (females), and 1 (6%) fish

with hemangiopericytoma (unknown sex). The liver of 1 fish (1%) collected at 2 weeks post exposure was lost during processing for histology. The rate of occurrence of the 5 histologic phenotypes observed at 2, 4, 6 and 10 weeks post-exposure is presented in figure 2. At 2 weeks post exposure, 3 (13%) male fish had no hepatic lesions, 3 (13%) males and 13 (57%) females had hepatocellular degenerative changes, and 4 (17%) males had BPDEC hyperplasia. At 4 weeks post exposure, 1 (4%) male fish had a normal liver, 2 (8%) females had evidence of hepatocellular degeneration, 7 (29%) males and 1 (4%) female had BPDEC hyperplasia and 13 (54%) females had hepatic fibrosis. At 6 weeks post exposure, 4 (17%) females had hepatocellular degenerative changes, 4 (17%) males had BPDEC hyperplasia, 2 (8%) males and 12 (50%) females had hepatic fibrosis and 2 (8%) females had hepatic neoplasms on a background of hepatic fibrosis. At 10 weeks post exposure, 3 (12%) males had BPDEC hyperplasia, 4 (17%) males and 3 (12%) females had hepatic fibrosis, and 5 (21%) males and 9 (38%) females had hepatic neoplasms.

Following DMN exposure there was a defined temporal progression towards fibrosis and neoplasia. First hepatocellular degeneration was observed, followed by BPDEC hyperplasia, hepatic fibrosis, and ultimately hepatic fibrosis with neoplasia. Females progressed faster to hepatic fibrosis and neoplasia than did males (i.e., males lagged by approximately 2 weeks, data not shown) as reported previously for neoplasia following diethylnitrosamine exposure (Teh and Hinton, 1998).

Transmission electron microscopy

To confirm that the HSC acquired fibroblast-like characteristics and that collagen was the extracellular matrix (ECM) deposited, control and fibrotic livers were examined by TEM. In control livers, cells with HSC morphologic characteristics were extremely rare and no cells demonstrated fibroblast-like features. However, in fibrotic livers, HSC were more frequent. Cells with HSC morphologic characteristics were located adjacent to collagen fibrils, and these cells had acquired myofibroblast characteristics such as cytoplasmic intermediate filament bundles, loss of lipid vacuoles and occasional presumptive collagen secretion granules (Fig. 3). Collagen fibrils in the space of Disse were very rare in control livers but frequently observed in fibrotic livers.

Morphometry

Muscle specific actin—Morphometric quantitation of MSA immunolabeling was used as a measure of stellate cell myofibroblastic transdifferentiation (Fig. 4). Liver sections from 22 controls, 12 phenotype 1, 8 phenotype 2, 16 phenotype 3 and 12 phenotype 4 had adequate MSA immunohistochemical labeling for morphometric analysis. The relationship between phenotype and the percent area occupied by the MSA immunoreactive cells is presented in figure 5. The percent area of MSA staining was significantly different between phenotypes except between control and phenotype 1 (hepatic degeneration) ($P < .05$). All MSA-positive cells were included for the morphometric analysis although a significant number were likely myofibroblasts. Cells located in the hepatic parenchyma and immunoreactive for MSA were interpreted as activated stellate cells. Cells closely surrounding bile ducts were interpreted as myofibroblasts. In control liver, MSA-positive cells were only observed closely surrounding bile ducts.

Masson's trichrome staining—Morphometric quantitation of Masson's trichrome staining was performed as a measure of collagen deposition and fibrosis (Fig. 6). Liver sections from 22 controls, 12 phenotype 1, 9 phenotype 2, 17 phenotype 3 and 12 phenotype 4 samples had adequate Masson's trichrome staining for morphometric analysis. The relationship between phenotype and the fibrosis score is presented in figure 8. The fibrosis scores were significantly different between all phenotypes. The MSA percentage area was significantly correlated with the fibrosis score ($P < .05$, $r = .903$)

Gene expression

Gene expression levels were determined only in liver samples that exceeded quality control (RIN) value for mRNA quality, and had sufficient amounts of tissue for morphometric analysis: 25 controls, 12 phenotype 1, 9 phenotype 2, 18 phenotype 3 and 12 phenotype 4 samples were evaluated. Messenger RNA expression levels of multiple fibrosis related genes were evaluated in relation to the liver phenotypes (Fig. 7). Change in expression of the following genes significantly correlated with the fibrosis score in phenotypes 1 and 2: tgfb1, tgfbr2, mmp2, mmp14a, mmp14b, timp2a, timp3, col1a1a, and col1a1b (($P < .05$, $r > .99$). At later time points, when fibrosis was established and continued to progress (phenotype 3 and 4), the expression levels of the genes listed above remained elevated but were lower than observed in phenotype 2, and therefore, correlation between gene expression level and fibrosis score was lost. No correlation was observed between gene expression of tgfbr1, smad3a, smad3b, col4a1, mmp13, timp2b, myc, ctnnb1 and fibrosis score in phenotype 1 and 2 livers.

TGF-β1 localisation

Immunohistochemistry was used to localize cells producing TGF-β1. In control and exposed livers with phenotype 1, TGF-β1-immunolabelling was present diffusely in the cytoplasm of cholangiocytes forming bile ducts, the BPDECs that were scattered along the biliary canaliculi and few scattered macrophages (Fig. 8 and 9). In exposed livers displaying phenotype 2 to 4, the number of cells immunolabeled with TGF-β1 was markedly increased due mainly to hypertrophy and hyperplasia of BPDECs lining biliary canaliculi and bile duct hyperplasia. Cholangiocytes and BPDECs were strongly immunoreactive. Weak to moderate positivity was present in a small number of macrophages. Occasional intermediate hepatocytes were weakly positive. No immunoreactivity for TGF- β1 was detected in the population of small elongated cells resembling rodent oval cells in the BPDEC hyperplasia phenotype (phenotype 2). TGF- β1 immunoreactivity was detected in all neoplasms. Most neoplastic hepatocytes had weak to moderate cytoplasmic immunoreactivity while neoplastic cholangiocytes were consistently strongly positive (Fig. 10 and 11). In order to confirm the identity of the non-hepatocyte cells expressing TGF-β1 in the hepatic parenchyma, labeling of consecutive tissue sections as well as double immunolabelling for CK, MSA and TGF-β1 was performed. Most cells immunolabeled with TGF-β1 and located in between hepatocytes were positive for CK but negative for MSA, thus supporting the notion that they are BPDECs. A smaller number of MSA-positive cells, often located along sinusoids, and interpreted as activated HSCs, were also positive for TGF-β1 (Fig. 8 and 9).

DISCUSSION

The use of small fish models in biomedical and environmental research continues to expand. In order to utilize these models to their full potential it is imperative to understand the similarities and differences in disease mechanisms among human, mammalian and fish models. The anatomical and histological differences between mammalian and piscine liver have been thoroughly studied in several species and especially the Japanese medaka (Hardman et al., 2007; Hardman et al., 2008). Medaka have a single lobed liver with microvasculature resembling a single mammalian hepatocytic lobule making it an ideal model to study the effects of hepatotoxicant (Hardman et al., 2007). Yet, our understanding of the piscine response to injury at the molecular level remains limited.

Hepatic fibrosis is a common wound-healing response to chronic liver injuries in mammals but is less often observed in fish (Wolf and Wolfe, 2005). Liver fibrosis has however been described in medaka exposed to DMN and methylazoxymethanol acetate (MAM-Ac) (Hatanaka et al., 1982; Hobbie et al., 2011). In this study, the expressions of key genes in the pathogenesis of hepatic fibrosis were associated with morphological changes that occurred during development of hepatic fibrosis/cirrhosis in DMN-exposed medaka. The DMN exposure protocol used in this study reliably produced morphological liver changes similar to those reported in medaka or observed in rodent models of hepatic fibrosis such as the DMN-induced rat model (Wallace et al., 2008; Hobbie et al., 2011). Progression to neoplasia was much faster in medaka than in rodents with neoplasia present in 8% and 67% of the fish collected at 6 and 10 weeks post exposure, respectively (Peto et al., 1991).

Females progressed faster to hepatic fibrosis and neoplasia than did males by approximately 2 weeks. This faster progression of hepatic lesions has been reported previously for neoplasia in several fish species, including medaka, and is considered a response to the promoter effect of endogenous steroids (Teh and Hinton, 1998; Cooke and Hinton, 1999). Estrogen has been demonstrated to have a significant effect on hepatocyte metabolism and to stimulate hepatic cell proliferation (Cooke and Hinton, 1999). Fibrogenesis in the liver is known to be subject to gonadal steroids influence; however the faster progression to fibrosis in medaka is opposite to the effect of estrogen in rodent and human where estrogen was associated with decreased fibrogenesis (Yasuda et al., 1999). The cause for this difference is uncertain. Given the anatomical and functional differences between medaka and mammalian livers, some lesion patterns expected in mammals were absent, such as centrilobular necrosis and bridging fibrosis (Hinton et al., 2008). Zonal necrosis patterns are not observed in fish as they lack hepatocellular metabolic zonation. Because the entire medaka liver is approximately the anatomical equivalent of one mammalian hepatic lobule, the biliary-venous tracts (portal tract equivalent) of fish are located mainly near the hilus and rarely in the parenchyma. Consequently, the type of bridging fibrosis observed in mammalian liver would be unexpected for fish (Hardman et al., 2007). The pattern of fibrosis that best characterizes the fibrotic changes observed in medaka is pericellular (perisinusoidal) fibrosis. In pericellular fibrosis, the collagenous matrix extends along the sinusoids and surrounds single or small groups of hepatocytes resulting in a chicken wire or latticework appearance.

In mammals, liver injury is associated with an increase in HSC numbers and the acquisition by the quiescent HSCs of a myofibroblast-like phenotype. The activated HSCs express smooth muscle α-actin (α-SMA) and acquire contractile properties. In human and rodent livers, immunohistochemistry for α-SMA is considered the gold standard to identify and localize activated HSC and myofibroblasts, and used as a marker of active fibrogenesis (Hautekeete and Geerts, 1997; Kweon et al., 2001). In medaka, perisinusoidal cells have been shown by immunohistochemistry (IHC) to express actin in fibrotic liver induced by DMN and hepatocellular carcinoma induced by DMN, diethylnitrosamine (DEN) or MAM-Ac. The lack of immunoreactivity with mammalian α-SMA antibodies necessitated our use of an antibody for MSA (Bunton, 1995; Hobbie et al., 2011).

In this study, evaluation of control and fibrotic liver by TEM confirmed that HSCs were more numerous in fibrotic livers and had acquired fibroblast-like characteristics, thus supporting the MSA staining results. Additionally, an increased amount of collagen fibrils, observed in the perisinusoidal spaces of fibrotic livers, supported the observations of H&E and Masson's trichrome stained liver sections. We quantified the amount of actin-positive cells following DMN injury and demonstrated a significant increase in actin-positive cell numbers that correlated with the development and progression of fibrosis determined on H&E and Masson's trichrome slides. These results indicate that the medaka liver response is similar to that observed in mammals where HSCs acquire a fibroblast-like phenotype and proliferate in fibrotic livers. We did not attempt to separate actin-positive cells (activated HSCs and myofibroblasts/smooth muscle cells) for morphometric analysis. The surface of all MSA positive cells was used for the analysis. Therefore, it was not determined if the increased number of actin-positive cells resulted from an increase in activated HSCs alone or in combination with an increase in myofibroblasts. We regard an increase in both activated HSCs and myofibroblasts as most likely.

We next examined expression of a number of genes associated with TGFβ signaling and deposition of ECM. Teleost fish often have two or more copies of single-copy mammalian genes (Postlethwait, 2007). The reason is presently unresolved but the whole genome duplication theory appears to be the most concrete explanation for teleostean gene duplication (Postlethwait, 2007). In this study we evaluated the expression levels of both gene copies when present including: *col1a1a*, and *col1a1b; smad3a* and *smad3b; mmp14a* and *mmp14b*.

Overall, expression of target genes exhibited a moderate increase in transcription during the early stage of hepatic degeneration (phenotype 1) and was followed by a marked increase in expression peaking when BPDEC hyperplasia (phenotype 2) occurred. Subsequently, gene expression decreased but remained significantly elevated when fibrosis (phenotype 3) was established and neoplasm(s) (phenotype 4) were developing.

In mammals, the TGF-β pathway is central in mediating fibrotic responses by regulating ECM production and resorption, and cellular proliferation. TGF-β1 is a potent antiproliferative cytokine that suppresses the proliferation of epithelial cells, including hepatocytes, and regulates the function of HSCs (Gressner et al., 2002). TGF-β signaling stimulates the synthesis of ECM components, such as type I, type III and type IV collagen

and reduces ECM degradation by up-regulating the expression of antiproteases such as TIMP-1 (Gressner et al., 2002).

Our data showed that activation of the TGF-β pathway occurs in medaka liver after hepatic injury. Increased *tgfb1* expression correlated with activation of HSCs and abnormal connective tissue deposition during onset and progression of fibrosis. A significant increase in expression of *tgfb1* and *tgfbr2* was accompanied by a delayed and lesser increase in *smad3a*, and *smad3b* expression. Expression of *tgfbr1* remained unchanged. Since the type II receptor is critical in receptor activation by binding the TGF-β ligand and activating TGFbRI, the increase in *tgfbr2* would presumably amplify activation of the TGF-β pathway. Similarly, *tgfbr2* is up-regulated in other fibrotic diseases such as in glomerulosclerosis and tubulointerstitial fibrosis of diabetic nephropathy, wound healing disorders, and keloid formation (Chin et al., 2001; Hong et al., 2001; Schultze-Mosgau et al., 2003). In patients with chronic liver disease, Calabrese et al., found an increase in expression of TGFBR2 with colocalization of TGF-β1 and SMAD on hepatocytes that correlated with an increased fibrosis score. Additionally, impairing the TGF-β pathway in rats exposed to DMN using an adenoviral vector expressing a truncated TGFR2 resulted in a marked reduction in hepatic fibrosis (Qi et al., 1999). However, Roulot et al., found that fibrotic livers in humans and rats exhibited a decrease in *Tgfbr2* expression and an increase in *Tgfbr1* expression in correlation with proliferation of HSCs and increased fibrosis (Roulot et al., 1999). These data suggest that there remains an inconsistent expression profile with TGF-β signaling and correlation to fibrosis in mammals.

We also observed a significant increase in *Smad3a* and *smad3b* levels within BPDEC hyperplasia and fibrotic livers, however, the fold induction was much lower than observed with *tgfb1* or *tgfbr2*. We chose to examine *Smad3* expression due to previous studies in mammals that demonstrated pro-fibrotic activities of TGF-β were mediated by SMAD3 in several organs including liver (Flanders, 2004; Roberts et al., 2006). The significant but lower change in *Smad3* expression is likely due to the fact that TGF-β1 stimulation of *Smad3* is mediated mostly through an increase in SMAD3 phosphorylation rather than a modification in *smad3* mRNA expression.

The TGF-β pathway is implicated in a number of cancers, including hepatic neoplasms. In the early stage of carcinogenesis, the TGF-β pathway acts as a tumor suppressor, but later it acts as a tumor promoter (Wakefield and Roberts, 2002; Musch et al., 2005; Mamiya et al., 2010). The results of this study suggest that upregulation of the TGF-β canonical pathway occurs in the fish liver neoplasms as is observed in spontaneous mouse and human HCC. In medaka, immunoreactivity for TGF- β1 was present in the neoplastic cells and the expression of *tgfb1, tgfbr2,* and *smad3a* remained upregulated in the fibrotic livers with neoplasms. We did not separate neoplastic tissue from fibrotic liver tissue during mRNA isolation. Therefore the expression level measured herein is not representative of the neoplasms alone and a definitive conclusion regarding the upregulation of the TGF-β pathway in these liver carcinomas cannot be made.

Expression and localization of *tgfbr2* is also known to be altered in cancer. However, its role remains unclear and expression has been shown to be increased, unchanged or decreased in

HCC in humans or in rodent models (Kiss et al., 1997; Abou-Shady et al., 1999; Mamiya et al., 2010; Hoenerhoff et al., 2011). In the present study, *tgfbr2* remained upregulated when neoplasms developed in the fibrotic liver.

The trend in expression levels of *tgfb1* and *tgfbr2* paralleled those of *col1a1a, col1a1b,* and to a lesser extent of *col4a1*.Upregulation of *tgfb1, tgfbr2, col1a1a, and col1a1b* correlated with activation of HSCs and deposition of ECM. Our findings are in accordance with those in humans and mammalian models in which increased collagen gene expression and deposition of collagen in hepatic fibrosis accompanies increased TGF-β1 production (Gressner et al., 2002).

Localization of TGF-β1 in fibrotic livers demonstrated protein expression in all BPDECs, cholangiocytes, some macrophages, and HSCs, and rarely in intermediate hepatocytes. These results are consistent with those of previously reported studies in medaka and in rats after hepatic injury (Jakowlew et al., 1991; Milani et al., 1991; Tao et al., 2000; Hobbie et al., 2011). They suggests that in fish, like in mammals, resident and recruited inflammatory cells (macrophages and Kupffer cells) and proliferating biliary epithelial cells promote fibrogenesis through increased production of TGF- β1 (Roth et al., 1998; Chantal, 2000; Matsuzaki, 2009). Although the antibody used in this study is sold as an anti-TGF-β1 antibody, the manufacturer states that it cross-reacts with TGF-β2. Given that its specificity in fish species is unknown, it is possible that the immunoreactivity observed in the cholangiocytes and BPDECs is due to TGF-β2 and not TGF-β1. Expression of *Tgfb2* mRNA is known to occur in cholangiocytes of proliferating bile ducts in rat and human fibrotic liver (Milani et al., 1991). It is interesting to note that Kupffer cells, an important source of TGF-β1 after hepatic injury in mammals, are absent in medaka and in most teleosts (Hardman et al., 2007; Hinton et al., 2008). However, fish livers often have interhepatocytic, perisinusoidal macrophages (IPM) that increase in number and phagocytize cellular debris following hepatic injury (Boorman et al., 1997; Okihiro and Hinton, 1999; Okihiro and Hinton, 2000). Given that immunoreactivity for TGF-β1 of some IPM was observed in this study, it is possible that IPM play a role similar to Kupffer cells in the pathogenesis of hepatic fibrogenesis.

A significant increase in expression of *mmp2, mmp14a, mmp14b, timp2a, timp2b,* and *timp3* was observed during development of hepatic fibrosis and neoplasia. A much smaller but significant increase in *mmp13* was also present. Trends in expression levels of the MMP and TIMP genes evaluated were paralleled by the upregulation of other genes typically expressed in fibrosis like *tgfb1* and *col1a1*. These results are similar to those reported in human and rodent studies where *Mmp2* and *M*mp*14* expression levels gradually increase with disease progression while the increase in *Mmp13* expression is transient, taking place mainly during the early phase of fibrosis and during recovery from fibrosis (Watanabe et al., 2000; Lichtinghagen et al., 2003; Hemmann et al., 2007). Expression of *Timp*-1, 2 and 3 also increased following liver injury in humans and rodents and persisted as fibrosis progressed (Iredale et al., 1996; Herbst et al., 1997; Kossakowska et al., 1998; Yoshiji et al., 2000). TIMP1 is the collagenase inhibitor most often evaluated in human and rodent studies and is considered an essential player in the development of hepatic fibrosis. Unfortunately, we were not able to identify an orthologous gene in the medaka genome.

The results suggest that this part of the pathogenesis in the medaka model is likely similar to the one in mammals where activation of the TGF-β pathways and HSCs results in alteration in the balance between production and resorption of ECM components. The net accumulation of collagen results predominantly from increased in transcription of collagen genes, mainly type I collagen, and impaired degradation due to changes in the balance between MMPs and TIMPs (Kossakowska et al., 1998; Hemmann et al., 2007). Studies of fibrosis in various organs including the liver indicate that an increase in the TIMP/MMP ratio promotes fibrosis (Iredale et al., 1996; Yoshiji et al., 2000; Madtes et al., 2001; Nicholson et al., 2002).

The Wnt signaling pathway has been implicated in organ fibrosis, including liver fibrosis, and neoplasia (Shackel et al., 2001; Kim et al., 2005; Myung et al., 2007). There is evidence that the profibrogenic role of Wnt signaling occurs through HSC activation and promotion of survival (Myung et al., 2007; Cheng et al., 2008). However, the role of the Wnt pathway in hepatic fibrosis is still poorly understood compared to its role in hepatic neoplasia (Thompson and Monga, 2007). β-catenin is the chief downstream effector of the canonical Wnt signaling pathway. In this study, we observed upregulation of *ctnnb1* suggesting upregulation of the Wnt canonical pathway during development and progression of hepatic fibrosis as it has been shown in mammals (Shackel et al., 2001; Myung et al., 2007; Cheng et al., 2008). However, we did not evaluate whether nuclear translocation of β-catenin occurred to provide direct evidence and confirm activation of the canonical Wnt pathways in this fish model. Additionally, *ctnnb1* upregulation was observed in fibrotic medaka liver with neoplasia suggesting that dysregulation of the Wnt pathway may occur in medaka liver carcinomas. Dysregulation of the Wnt pathway with overexpression of the β-catenin protein is an important factor in the development and progression of HCCs in zebrafish, rodents and humans (Harada et al., 2004; Haramis et al., 2006; Kim et al., 2008). However, HCCs were not separated from the surrounding fibrotic liver and it cannot be determined if this increase is part of the fibrotic process or HCC development or both.

MYC, a ubiquitous transcription factor regulates transcription of numerous genes involved in functions that control cell proliferation and differentiation (Oster et al., 2002). Up-regulation of *Myc* follows activation of various mitogenic signaling pathways including the Wnt pathway. In this study, *myc* was up-regulated in all phenotypes evaluated including livers containing neoplasms. This finding suggests possible roles in hepatocyte proliferation and neoplasia in medaka. Temporary up-regulation of *Myc* is known to occur during hepatic regeneration while sustained up-regulation is linked to neoplasia in rodents and humans (Santoni-Rugiu et al., 1996; Michalopoulos and DeFrances, 1997). Sustained *myc* expression in hepatocytes of transgenic zebrafish and medaka overexpressing *myc* resulted in hyperplasia and, in zebrafish only, possible hepatocellular adenoma (Gong et al., 2011; Menescal et al., 2012).

This medaka fish fibrosis model has the potential to be a valuable tool to study development and progression of fibrosis and liver cancer *in vivo* and help bridge the gap between *in vitro* and *in vivo* testing. Small size, economy, ease of use of large numbers of individuals, low background incidence of neoplasia, and rapid induction of fibrosis and neoplasia are some characteristics of this model that make it amendable for high throughput screening of novel

therapeutic drugs and identification of novel regulatory pathways. The availability of the medaka transparent fish strains STII and STIII, one of the only two vertebrate animal models which are transparent in larval and adult stage, opens the possibility to study tissue responses and gene expressions non-invasively *in vivo* (Hardman et al., 2008). Genetic manipulation such as precise genetic gain- and loss-of-function studies or generation of transgenic fish with spatio-temporal cre-lox transgene regulation may also facilitate study of the molecular pathogenesis of fibrosis. However, we allege that a carcinogen-induced model of hepatic fibrosis and neoplasia will not absolutely recapitulate the pathogenesis of the human disease. In this model the primary initiating event is a protein and DNA-damaging episode (DMN exposure) that results in fibrosis, cirrhosis and development of neoplasms within a few weeks rather than a repetitive toxic or viral hepatic injury that progress slowly over decades as in human.In conclusion, the results of this study demonstrate that the principal cellular and molecular events in the pathogenesis of DMN-induced hepatic fibrosis in mammals and medaka fish are conserved. Hepatocellular injury is followed by activation of HSCs, TGF-β pathway activation, change in the balance between MMPs and TIMPs and an increase in collagen production with the end result of excessive deposition of collagenous ECM. These data also support the medaka as a useful alternative animal model of hepatic fibrosis and improves the comparative understanding of the liver's response to chronic injury across taxa.

Acknowledgments

The authors wish to thank Dr. John Cullen for his valuable comments on the results interpretation. We are also grateful to Sandra Horton, Monica Matmeuller, and the staff of the Histopathology Laboratory as well as Jeanette Shipley-Phillips from the Laboratory for Advanced Electron and Light Optical Methods at the NCSU-CVM for their expertise. We also thank Shashi Gadi for help with the medaka maintenance and Dr. Jason Osborne from the NCSU Department of Statistics. This manuscript is submitted in partial fulfillment of the degree of Doctor of Philosophy to Dr. Arnaud Van Wettere.

Abbreviations

AP	alkaline phosphatase
BPDEC	bile preductular epithelial cell
CC	cholangiocarcinoma
CHC	combined hepatocellular-cholangiocarcinoma
CK	pancytokeratin
COL1A1	collagen type I alpha 1
COL4A1	collagen type IV alpha 1
CTNNB1	beta-catenin
DAB	3,3-diaminobenzidine
DMN	dimethylnitrosamine
ECM	extracellular matrix
HCC	hepatocellular carcinoma

H&E	hematoxylin and eosin
HRP	horseradish peroxidase
HSC	hepatic stellate cells
INHAND	international harmonization of nomenclature and diagnostic criteria for lesions in rats and mice
MAM-Ac	methylazoxymethanol acetate
MMP	matrix metalloproteinases
MSA	muscle specific actin
NCSU	North Carolina state university
PBS	phosphate-buffered saline
qPCR	quantitative polymerase chain reaction
RIN	RNA integrity number
RO	reverse osmosis
α-SMA	smooth muscle α-actin
SMAD3	mothers against decapentaplegic homolog 3
TEM	transmission electron microscopy
TGF-β	transforming growth factor beta
TGFbR	transforming growth factor beta receptor
TIMP	tissue inhibitors of metalloproteinases

REFERENCES

Abou-Shady M, Baer HU, Friess H, Berberat P, Zimmermann A, Graber H, Gold LI, Korc M, Buchler MW. Transforming growth factor betas and their signaling receptors in human hepatocellular carcinoma. Am J Surg. 1999; 177:209–15. [PubMed: 10219856]

Ala-Kokko L, Pihlajaniemi T, Myers JC, Kivirikko KI, Savolainen ER. Gene expression of type I, III and IV collagens in hepatic fibrosis induced by dimethylnitrosamine in the rat. Biochem J. 1987; 244:75–9. [PubMed: 3663119]

Boorman GA, Botts S, Bunton TE, Fournie JW, Harshbarger JC, Hawkins WE, Hinton DE, Jokinen MP, Okihiro MS, Wolfe MJ. Diagnostic Criteria for Degenerative, Inflammatory, Proliferative Nonneoplastic and Neoplastic Liver Lesions in Medaka (*Oryzias latipes*): Consensus of a National Toxicology Program Pathology Working Group. Toxicol Pathol. 1997; 25:202–10. [PubMed: 9125779]

Bunton TE. Expression of actin and desmin in experimentally induced hepatic lesions and neoplasms from medaka (*Oryzias latipes*). Carcinogenesis. 1995; 16:1059–63. [PubMed: 7767965]

Calabrese F, Valente M, Giacometti C, Pettenazzo E, Benvegnu L, Alberti A, Gatta A, Pontisso P. Parenchymal transforming growth factor beta-1: its type II receptor and Smad signaling pathway correlate with inflammation and fibrosis in chronic liver disease of viral etiology. J Gastroenterol Hepatol. 2003; 18:1302–8. [PubMed: 14535988]

Chantal H. Biliary epithelial cell response to cholestasis. J Hepatol. 2000; 32(Supplement 2):14–5.

Cheng JH, She H, Han YP, Wang J, Xiong S, Asahina K, Tsukamoto H. Wnt antagonism inhibits hepatic stellate cell activation and liver fibrosis. Am J Physiol Gastrointest Liver Physiol. 2008; 294:G39–49. [PubMed: 18006602]

Chin GS, Liu W, Peled Z, Lee TY, Steinbrech DS, Hsu M, Longaker MT. Differential expression of transforming growth factor-beta receptors I and II and activation of Smad 3 in keloid fibroblasts. Plast Reconstr Surg. 2001; 108:423–9. [PubMed: 11496185]

Cooke JB, Hinton DE. Promotion by 17β-estradiol and β-hexachlorocyclohexane of hepatocellular tumors in medaka, *Oryzias latipes*. Aquat Toxicol. 1999; 45:127–45.

Dykstra, MJ. Manual of Applied Techniques for Biological Electron Microscopy. Plenum Press; New York, NY: 1993.

Flanders KC. Smad3 as a mediator of the fibrotic response. Int J ExpPathol. 2004; 85:47–64.

George J, Rao K,R, Stern R, Chandrakasan G. Dimethylnitrosamine-induced liver injury in rats: the early deposition of collagen. Toxicology. 2001; 156:129–38. [PubMed: 11164615]

Gong, Z.; Koh, CHV.; Nguyen, AT.; Zhan, H.; Li, Z.; Lam, SH.; Spitsbergen, JM.; Emelyanov, A.; Parinov, S. The Zebrafish Model for Liver Carcinogenesis. In: Wang, XW.; Grisham, JW.; Thorgeirsson, SS., editors. Molecular Genetics of Liver Neoplasia. Springer New York; New York, NY: 2011. p. 197-218.

Gressner AM, Weiskirchen R, Breitkopf K, Dooley S. Roles of TGF-beta in hepatic fibrosis. Front Biosci. 2002; 7:793–807.

Harada N, Oshima H, Katoh M, Tamai Y, Oshima M, Taketo MM. Hepatocarcinogenesis in mice with beta-catenin and Ha-ras gene mutations. Cancer Res. 2004; 64:48–54. [PubMed: 14729607]

Haramis AP, Hurlstone A, van der Velden Y, Begthel H, van den Born M, Offerhaus GJ, Clevers HC. Adenomatous polyposis coli-deficient zebrafish are susceptible to digestive tract neoplasia. EMBO Rep. 2006; 7:444–9. [PubMed: 16439994]

Hardman RC, Kullman SW, Hinton DE. Non invasive in vivo investigation of hepatobiliary structure and function in STII medaka (*Oryzias latipes*): methodology and applications. Comp Hepatol. 2008; 7:7. [PubMed: 18838008]

Hardman RC, Volz DC, Kullman SW, Hinton DE. An in vivo look at vertebrate liver architecture: three-dimensional reconstructions from medaka (*Oryzias latipes*). Anat Rec (Hoboken). 2007; 290:770–82. [PubMed: 17516461]

Hatanaka J, Doke N, Harada T, Aikawa T, Enomoto M. Usefulness and rapidity of screening for the toxicity and carcinogenicity of chemicals in medaka, *Oryzias latipes*. Jpn J Exp Med. 1982; 52:243–53. [PubMed: 7169669]

Hautekeete ML, Geerts A. The hepatic stellate (Ito) cell: its role in human liver disease. Virchows Arch. 1997; 430:195–207. [PubMed: 9099976]

Hemmann S, Graf J, Roderfeld M, Roeb E. Expression of MMPs and TIMPs in liver fibrosis - a systematic review with special emphasis on anti-fibrotic strategies. J Hepatol. 2007; 46:955–75. [PubMed: 17383048]

Herbst H, Wege T, Milani S, Pellegrini G, Orzechowski HD, Bechstein WO, Neuhaus P, Gressner AM, Schuppan D. Tissue inhibitor of metalloproteinase-1 and -2 RNA expression in rat and human liver fibrosis. Am J Pathol. 1997; 150:1647–59. [PubMed: 9137090]

Hernandez-Gea V, Friedman SL. Pathogenesis of Liver Fibrosis. Annu Rev Pathol. 2010; 6:456.

Heron M, Hoyert DL, Murphy SL, Xu J, Kochanek KD, Tejada-Vera B. Deaths: final data for 2006. Natl Vital Stat Rep. 2009; 57:1–134. [PubMed: 19788058]

Hinton D,E, Hardman R,C, Kullman S,W, Law JMM, Schmale M,C, Walter R,B, Winn R,N, Yoder J,A. Aquatic animal model of human disease: Selected papers and recommendations from the 4th Conference. Comp Biochem Physiol C Toxicol Pharmacol. 2009; 149:121–28. [PubMed: 19150511]

Hinton, DE.; Segner, H.; Au, DWT.; Kullman, SK.; Hardman, RC. Liver Toxicity. In: Di Giulio, RT.; Hinton, DE., editors. The Toxicology of Fishes. CRC Press; Boca Raton, FL: 2008. p. 401

Hobbie KR, Deangelo AB, George MH, Law JM. Neoplastic and Nonneoplastic Liver Lesions Induced by Dimethylnitrosamine in Japanese Medaka Fish. Vet Pathol. 2011; 49:372–85. [PubMed: 21724976]

Hoenerhoff MJ, Pandiri AR, Lahousse SA, Hong HH, Ton TV, Masinde T, Auerbach SS, Gerrish K, Bushel PR, Shockley KR, Peddada SD, Sills RC. Global Gene Expression Profiling of Spontaneous Hepatocellular Carcinoma in B6C3F1 Mice: Similarities in the Molecular Landscape with Human Liver Cancer. Toxicol Pathol. 2011; 39:678–99. [PubMed: 21571946]

Hong SW, Isono M, Chen S, Iglesias-De La Cruz MC, Han DC, Ziyadeh FN. Increased glomerular and tubular expression of transforming growth factor-beta1, its type II receptor, and activation of the Smad signaling pathway in the db/db mouse. Am J Pathol. 2001; 158:1653–63. [PubMed: 11337363]

Hyon M, Kwon E, Choi HJ, Kang B. Dimethylnitrosamine-Induced Liver Fibrosis and Recovery in NOD/SCID Mice. J Vety Med Sci. 2011; 73:739–45.

Iredale JP, Benyon RC, Arthur MJ, Ferris WF, Alcolado R, Winwood PJ, Clark N, Murphy G. Tissue inhibitor of metalloproteinase-1 messenger RNA expression is enhanced relative to interstitial collagenase messenger RNA in experimental liver injury and fibrosis. Hepatology. 1996; 24:176–84. [PubMed: 8707259]

Jakowlew SB, Mead JE, Danielpour D, Wu J, Roberts AB, Fausto N. Transforming growth factor-beta (TGF-beta) isoforms in rat liver regeneration: messenger RNA expression and activation of latent TGF-beta. Cell Regul. 1991; 2:535–48. [PubMed: 1782214]

Jezequel AM, Mancini R, Rinaldesi ML, Macarri G, Venturini C, Orlandi F. A morphological study of the early stages of hepatic fibrosis induced by low doses of dimethylnitrosamine in the rat. J Hepatol. 1987; 5:174–81. [PubMed: 3693862]

Kim Y, Sills RC, Houle CD. Overview of the molecular biology of hepatocellular neoplasms and hepatoblastomas of the mouse liver. Toxicol Pathol. 2005; 33:175–80. [PubMed: 15805069]

Kim YD, Park CH, Kim HS, Choi SK, Rew JS, Kim DY, Koh YS, Jeung KW, Lee KH, Lee JS, Juhng SW, Lee JH. Genetic alterations of Wnt signaling pathway-associated genes in hepatocellular carcinoma. J Gastroenterol Hepatol. 2008; 23:110–8. [PubMed: 18171349]

Kiss A, Wang NJ, Xie JP, Thorgeirsson SS. Analysis of transforming growth factor (TGF)-alpha/epidermal growth factor receptor, hepatocyte growth Factor/c-met,TGF-beta receptor type II, and p53 expression in human hepatocellular carcinomas. Clin Cancer Res. 1997; 3:1059–66. [PubMed: 9815784]

Kossakowska AE, Edwards DR, Lee SS, Urbanski LS, Stabbler AL, Zhang CL, Phillips BW, Zhang Y, Urbanski SJ. Altered balance between matrix metalloproteinases and their inhibitors in experimental biliary fibrosis. Am J Pathol. 1998; 153:1895–902. [PubMed: 9846979]

Kweon YO, Goodman ZD, Dienstag JL, Schiff ER, Brown NA, Burchardt E, Schoonhoven R, Brenner DA, Fried MW. Decreasing fibrogenesis: an immunohistochemical study of paired liver biopsies following lamivudine therapy for chronic hepatitis B. J Hepatol. 2001; 35:749–55. [PubMed: 11738102]

Lichtinghagen R, Bahr MJ, Wehmeier M, Michels D, Haberkorn CI, Arndt B, Flemming P, Manns MP, Boeker KH. Expression and coordinated regulation of matrix metalloproteinases in chronic hepatitis C and hepatitis C virus-induced liver cirrhosis. Clin Sci (Lond). 2003; 105:373–82. [PubMed: 12760742]

Livak KJ, Schmittgen TD. Analysis of relative gene expression data using real-time quantitative PCR and the 2(-Delta Delta C(T)) Method. Methods. 2001; 25:402–8. [PubMed: 11846609]

Madtes DK, Elston AL, Kaback LA, Clark JG. Selective induction of tissue inhibitor of metalloproteinase-1 in bleomycin-induced pulmonary fibrosis. Am J Respir Cell Mol Biol. 2001; 24:599–607. [PubMed: 11350830]

Mamiya T, Yamazaki K, Masugi Y, Mori T, Effendi K, Du W, Hibi T, Tanabe M, Ueda M, Takayama T, Sakamoto M. Reduced transforming growth factor-beta receptor II expression in hepatocellular carcinoma correlates with intrahepatic metastasis. Lab Invest. 2010; 90:1339–45. [PubMed: 20531292]

Matsuzaki K. Modulation of TGF-beta signaling during progression of chronic liver diseases. Front Biosci. 2009; 14:2923–34.

McDowell EM, Trump BF. Histologic fixatives suitable for diagnostic light and electron microscopy. Arch Pathol Lab Med. 1976; 100:405–14. [PubMed: 60092]

Menescal LA, Schmidt C, Liedtke D, Schartl M. Liver hyperplasia after tamoxifen induction of Myc in a transgenic medaka model. Dis Model Mech. 2012; 5:492–502. [PubMed: 22422827]

Michalopoulos GK, DeFrances MC. Liver regeneration. Science. 1997; 276:60–6. [PubMed: 9082986]

Milani S, Herbst H, Schuppan D, Stein H, Surrenti C. Transforming growth factors beta 1 and beta 2 are differentially expressed in fibrotic liver disease. Am J Pathol. 1991; 139:1221–9. [PubMed: 1750499]

Musch A, Rabe C, Paik MD, Berna MJ, Schmitz V, Hoffmann P, Nischalke HD, Sauerbruch T, Caselmann WH. Altered expression of TGF-beta receptors in hepatocellular carcinoma--effects of a constitutively active TGF-beta type I receptor mutant. Digestion. 2005; 71:78–91. [PubMed: 15775675]

Myung SJ, Yoon JH, Gwak GY, Kim W, Lee JH, Kim KM, Shin CS, Jang JJ, Lee SH, Lee SM, Lee HS. Wnt signaling enhances the activation and survival of human hepatic stellate cells. FEBS Lett. 2007; 581:2954–8. [PubMed: 17544413]

Nicholson ML, Waller JR, Bicknell GR. Renal transplant fibrosis correlates with intragraft expression of tissue inhibitor of metalloproteinase messenger RNA. Br J Surg. 2002; 89:933–7. [PubMed: 12081746]

Ohara F, Nii A, Sakiyama Y, Tsuchiya M, Ogawa S. Pathophysiological Characteristics of Dimethylnitrosamine-Induced Liver Fibrosis in Acute and Chronic Injury Models: A Possible Contribution of KLF5 to Fibrogenic Responses. Dig Dis Sci. 2007; 53:2222–32. [PubMed: 18095165]

Okihiro M,S, Hinton D,E. Partial hepatectomy and bile duct ligation in rainbow trout (*Oncorhynchus mykiss*): histologic, immunohistochemical and enzyme histochemical characterization of hepatic regeneration and biliary hyperplasia. Toxicol Pathol. 2000; 28:342–56. [PubMed: 10805153]

Okihiro MS, Hinton DE. Progression of hepatic neoplasia in medaka (*Oryzias latipes*) exposed to diethylnitrosamine. Carcinogenesis. 1999; 20:933–40. [PubMed: 10357770]

Oster SK, Ho CS, Soucie EL, Penn LZ. The myc oncogene: MarvelouslY Complex. Adv Cancer Res. 2002; 84:81–154. [PubMed: 11885563]

Parkin D,M, Bray F, Ferlay J, Pisani P. Estimating the world cancer burden: Globocan 2000. Int J Cancer. 2001; 94:153–6. [PubMed: 11668491]

Peto R, Gray R, Brantom P, Grasso P. Effects on 4080 rats of chronic ingestion of N-nitrosodiethylamine or N-nitrosodimethylamine: a detailed dose-response study. Cancer Res. 1991; 51:6415–51. [PubMed: 1933906]

Postlethwait JH. The zebrafish genome in context: ohnologs gone missing. J ExpZool B Mol Dev Evol. 2007; 308:563–77.

Qi Z, Atsuchi N, Ooshima A, Takeshita A, Ueno H. Blockade of type beta transforming growth factor signaling prevents liver fibrosis and dysfunction in the rat. Proc Natl Acad Sci U S A. 1999; 96:2345–9. [PubMed: 10051644]

Roberts AB, Tian F, Byfield SD, Stuelten C, Ooshima A, Saika S, Flanders KC. Smad3 is key to TGF-beta-mediated epithelial-to-mesenchymal transition, fibrosis, tumor suppression and metastasis. Cytokine Growth Factor Rev. 2006; 17:19–27. [PubMed: 16290023]

Roth S, Gong W, Gressner AM. Expression of different isoforms of TGF-beta and the latent TGF-beta binding protein (LTBP) by rat Kupffer cells. J Hepatol. 1998; 29:915–22. [PubMed: 9875638]

Roulot D, Sevcsik AM, Coste T, Strosberg AD, Marullo S. Role of transforming growth factor beta type II receptor in hepatic fibrosis: studies of human chronic hepatitis C and experimental fibrosis in rats. Hepatology. 1999; 29:1730–8. [PubMed: 10347115]

Santoni-Rugiu E, Preisegger KH, Kiss A, Audolfsson T, Shiota G, Schmidt EV, Thorgeirsson SS. Inhibition of neoplastic development in the liver by hepatocyte growth factor in a transgenic mouse model. Proc Natl Acad Sci U S A. 1996; 93:9577–82. [PubMed: 8790372]

Schultze-Mosgau S, Wehrhan F, Rödel F, Amann K, Radespiel-Tröger M, Grabenbauer GG. Transforming growth factor-β receptor-II up-regulation during wound healing in previously irradiated graft beds in vivo. Wound Repair Regen. 2003; 11:297–305. [PubMed: 12846918]

Shackel NA, McGuinness PH, Abbott CA, Gorrell MD, McCaughan GW. Identification of novel molecules and pathogenic pathways in primary biliary cirrhosis: cDNA array analysis of intrahepatic differential gene expression. Gut. 2001; 49:565–76. [PubMed: 11559656]

Sherman M. Hepatocellular carcinoma: epidemiology, surveillance, and diagnosis. Semin Liver Dis. 2010; 30:3–16. [PubMed: 20175029]

Tada S, Nakamuta M, Enjoji M, Sugimoto R, Iwamoto H, Kato M, Nakashima Y, Nawata H. Pirfenidone inhibits dimethylnitrosamine-induced hepatic fibrosis in rats. Clin Exp Pharmacol Physiol. 2001; 28:522–7. [PubMed: 11422218]

Tao LH, Enzan H, Hayashi Y, Miyazaki E, Saibara T, Hiroi M, Toi M, Kuroda N, Naruse K, Jin YL, Guo LM. Appearance of denuded hepatic stellate cells and their subsequent myofibroblast-like transformation during the early stage of biliary fibrosis in the rat. Med Electron Microsc. 2000; 33:217–30. [PubMed: 11810479]

Teh SJ, Hinton DE. Gender-specific growth and hepatic neoplasia in medaka (*Oryzias latipes*). Aquat Toxicol. 1998; 41:141–59.

Thompson MD, Monga SP. WNT/beta-catenin signaling in liver health and disease. Hepatology. 2007; 45:1298–305. [PubMed: 17464972]

Thoolen B, Maronpot RR, Harada T, Nyska A, Rousseaux C, Nolte T, Malarkey DE, Kaufmann W, Kuttler K, Deschl U, Nakae D, Gregson R, Vinlove MP, Brix AE, Singh B, Belpoggi F, Ward JM. Proliferative and nonproliferative lesions of the rat and mouse hepatobiliary system. Toxicol Pathol. 2010; 38:5S–81S. [PubMed: 21191096]

Wakefield LM, Roberts AB. TGF-beta signaling: positive and negative effects on tumorigenesis. CurrOpin Genet Dev. 2002; 12:22–9.

Wallace K, Burt AD, Wright MC. Liver fibrosis. Biochem J. 2008; 411:1–18. [PubMed: 18333835]

Watanabe T, Niioka M, Hozawa S, Kameyama K, Hayashi T, Arai M, Ishikawa A, Maruyama K, Okazaki I. Gene expression of interstitial collagenase in both progressive and recovery phase of rat liver fibrosis induced by carbon tetrachloride. J Hepatol. 2000; 33:224–35. [PubMed: 10952240]

Wolf JC, Wolfe MJ. A Brief Overview of Nonneoplastic Hepatic Toxicity in Fish. Toxicol Pathol. 2005; 33:75–85. [PubMed: 15805058]

Yasuda M, Shimizu I, Shiba M, Ito S. Suppressive effects of estradiol on dimethylnitrosamine-induced fibrosis of the liver in rats. Hepatology. 1999; 29:719–27. [PubMed: 10051473]

Yoshiji H, Kuriyama S, Miyamoto Y, Thorgeirsson UP, Gomez DE, Kawata M, Yoshii J, Ikenaka Y, Noguchi R, Tsujinoue H, Nakatani T, Thorgeirsson SS, Fukui H. Tissue inhibitor of metalloproteinases-1 promotes liver fibrosis development in a transgenic mouse model. Hepatology. 2000; 32:1248–54. [PubMed: 11093731]

Zhang Z, Hu J. Development and validation of endogenous reference genes for expression profiling of medaka (*Oryzias latipes*) exposed to endocrine disrupting chemicals by quantitative real-time RT-PCR. Toxicol Sci. 2007; 95:356–68. [PubMed: 17093204]

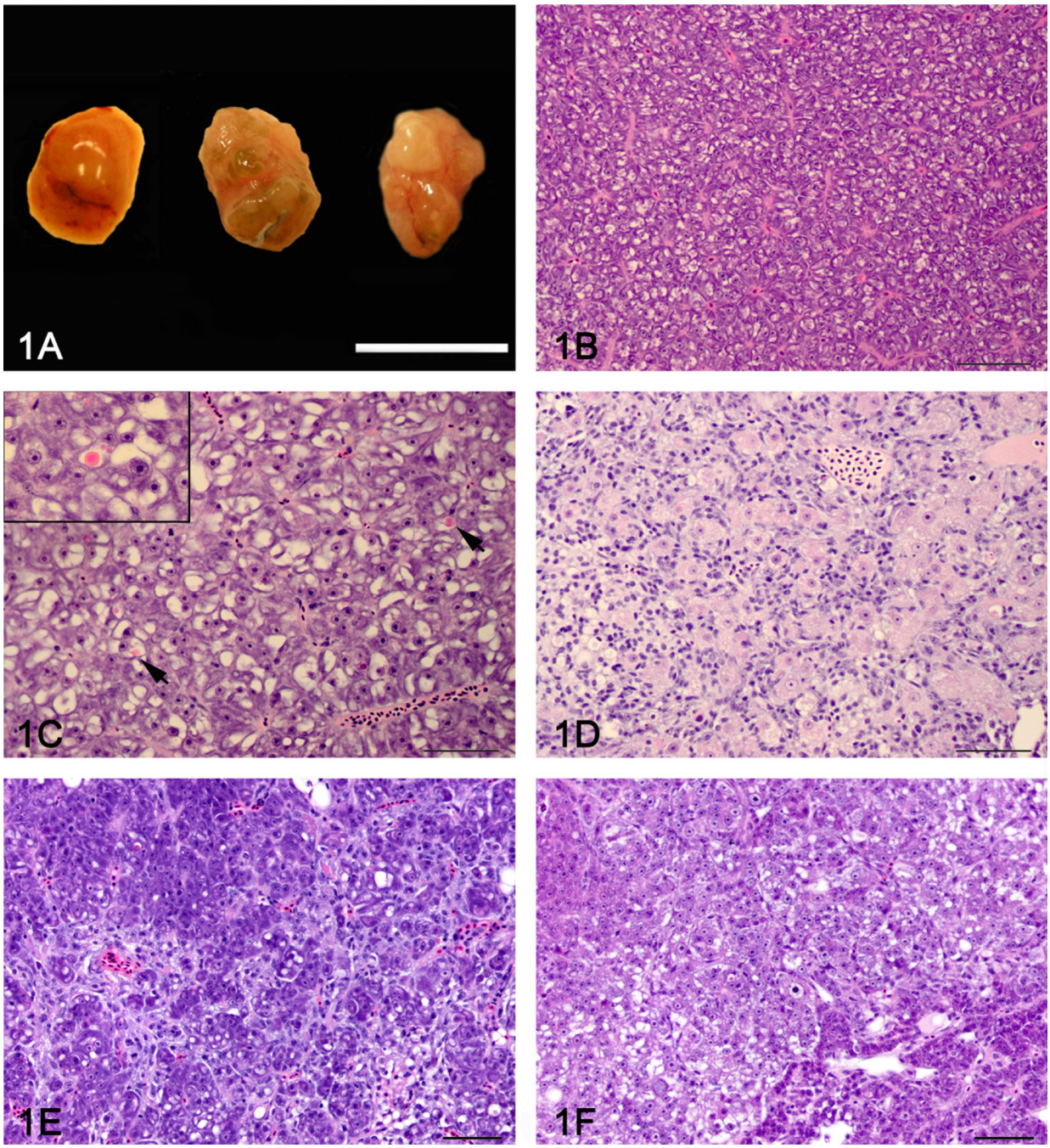

Figure 1.

Gross appearance and histology of control and DMN exposed liver A: Gross appearance of a normal medaka liver (left) and 2 livers with severe hepatic fibrosis (center and right). The liver on the right has a grossly visible neoplasm diagnosed as a hepatocellular carcinoma by histology. Bar = 1 mm. B: Histology of a normal female medaka liver (phenotype 0). C: Hepatocellular degeneration (phenotype 1) characterized by increased hepatocellular vacuolization, presence of globular eosinophilic intra-cytoplasmic inclusions (arrow) and scattered apoptotic hepatocytes. Insert: Close-up of an eosinophilic intra-cytoplasmic

inclusion. 100X. D: Biliary preductular epithelial cell hyperplasia (phenotype 2) characterized by proliferation of small cells with hyperchromatic elongated nuclei that separated the hepatocytes and sometimes surrounded individual hepatocytes. E: Hepatic fibrosis (phenotype 3) characterized by increase connective tissue separating and individualizing single or small group of hepatocytes. F: The hepatic fibrosis and neoplasia phenotype (phenotype 4) was defined as hepatic fibrosis with presence of a hepatic neoplasm (Hepatocellular carcinoma or cholangiocellular carcinoma). Hematoxylin and eosin. Bar = 50 μm 40X.

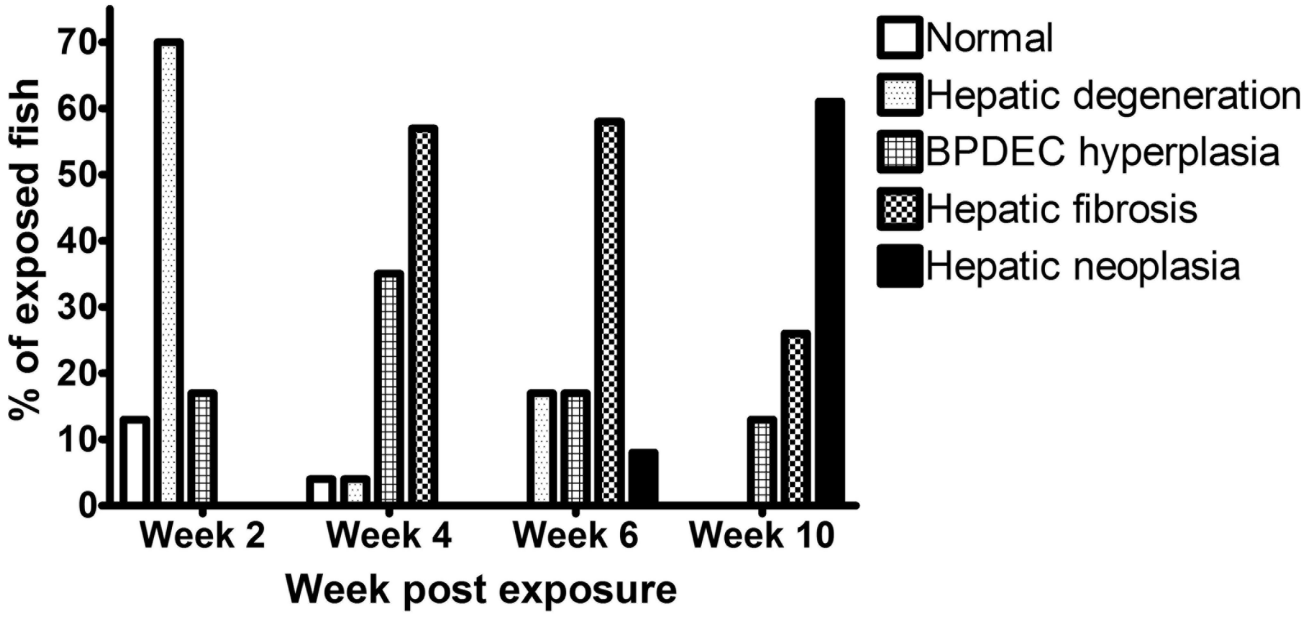

Figure 2.
Rate of occurrence of the 5 histologic liver phenotypes observed at the 2, 4, 6 and 10 weeks after DMN exposure.

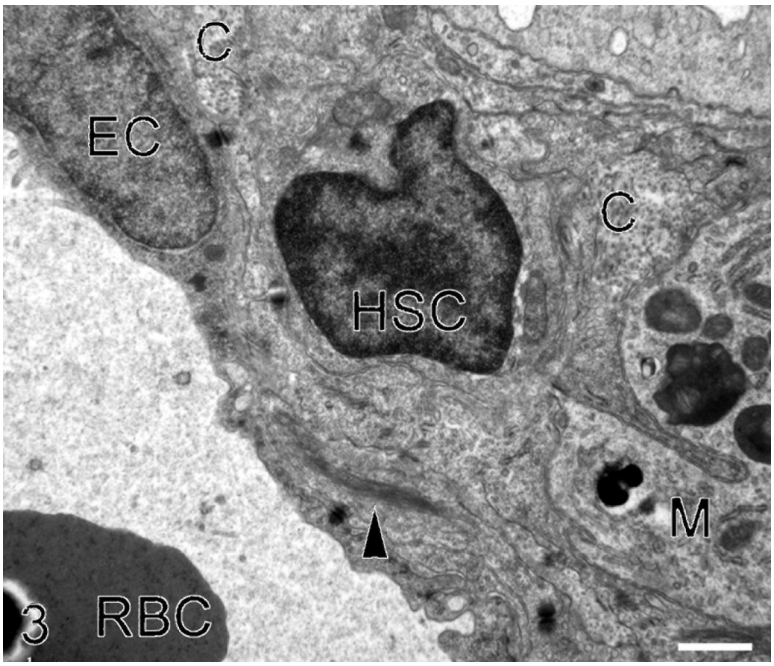

Figure 3.

Transmission electron microscopy of an activated hepatic stellate cell (HSC). Collagen fibrils (C) and a macrophage (M) are also present in the space of Disse. This HSC has lost its lipid vacuole(s) and a bundle of intermediate filaments (arrow head) is present in the cytoplasm. E: endothelial cell. RBC: red blood cell. Bar = 1 μm. X 8900.

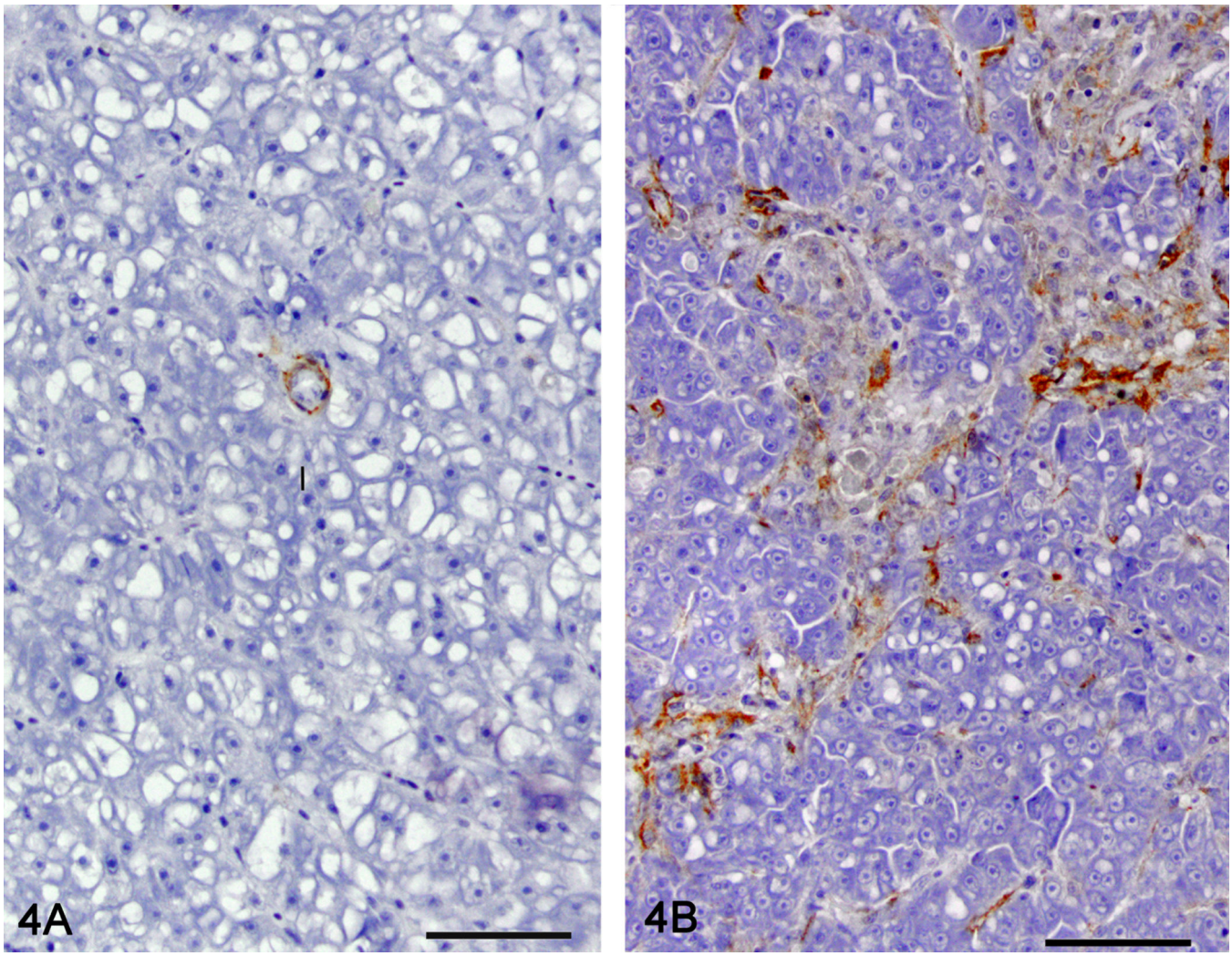

Figure 4.

Immunolabeling for MSA as a measure of stellate cell myofibroblastic transdifferentiation. Representative picture of a control liver (4A) and liver with hepatic fibrosis (4B). MSA immunohistochemistry, hematoxylin counterstain. Bar = 50 μm 40X.

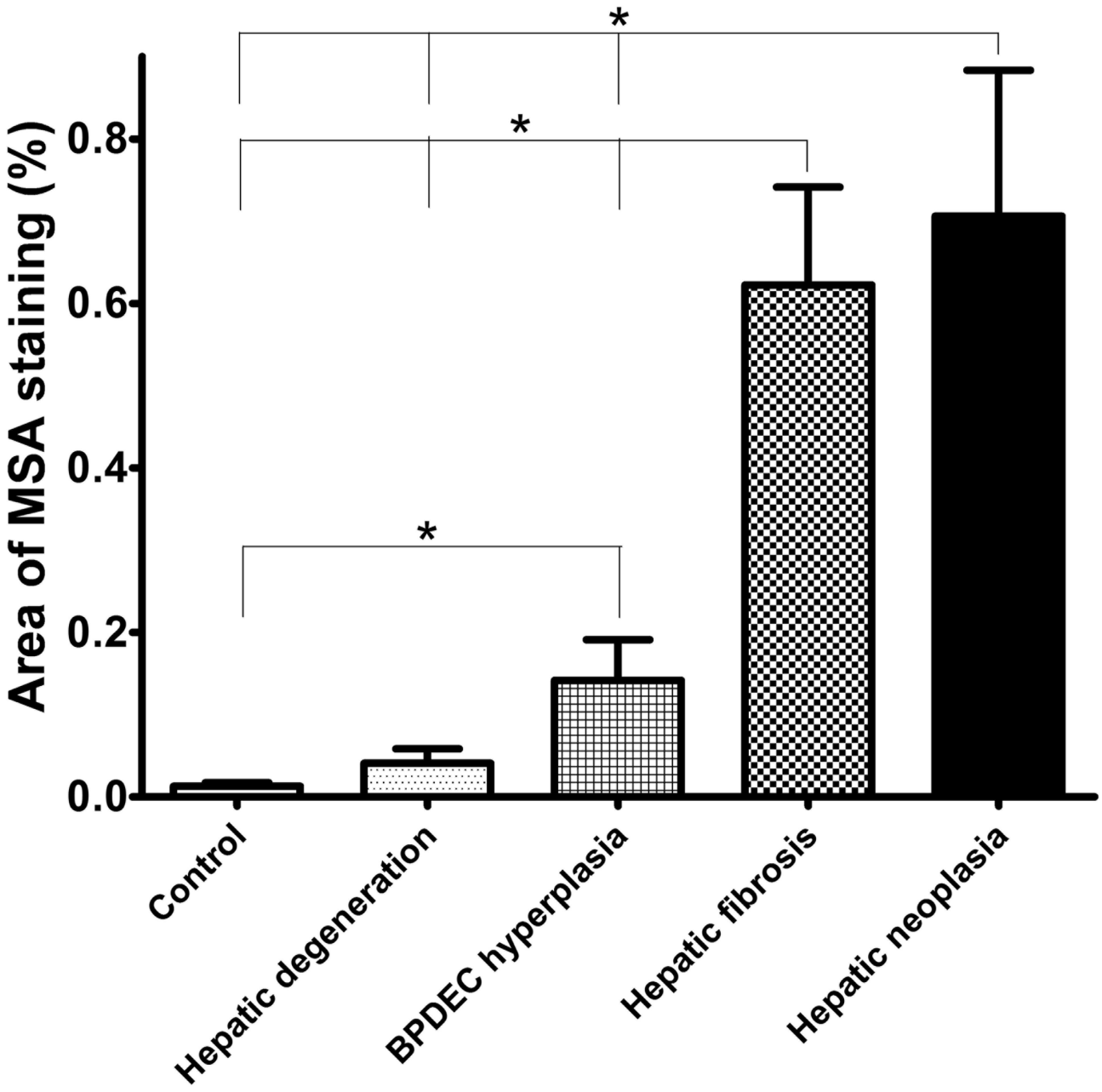

Figure 5.

Morphometric quantitation of MSA immunolabelling as a measure of stellate cell myofibroblastictrans differentiation. Relationship between phenotype and the area percentage occupied by the MSA immunostained cells.

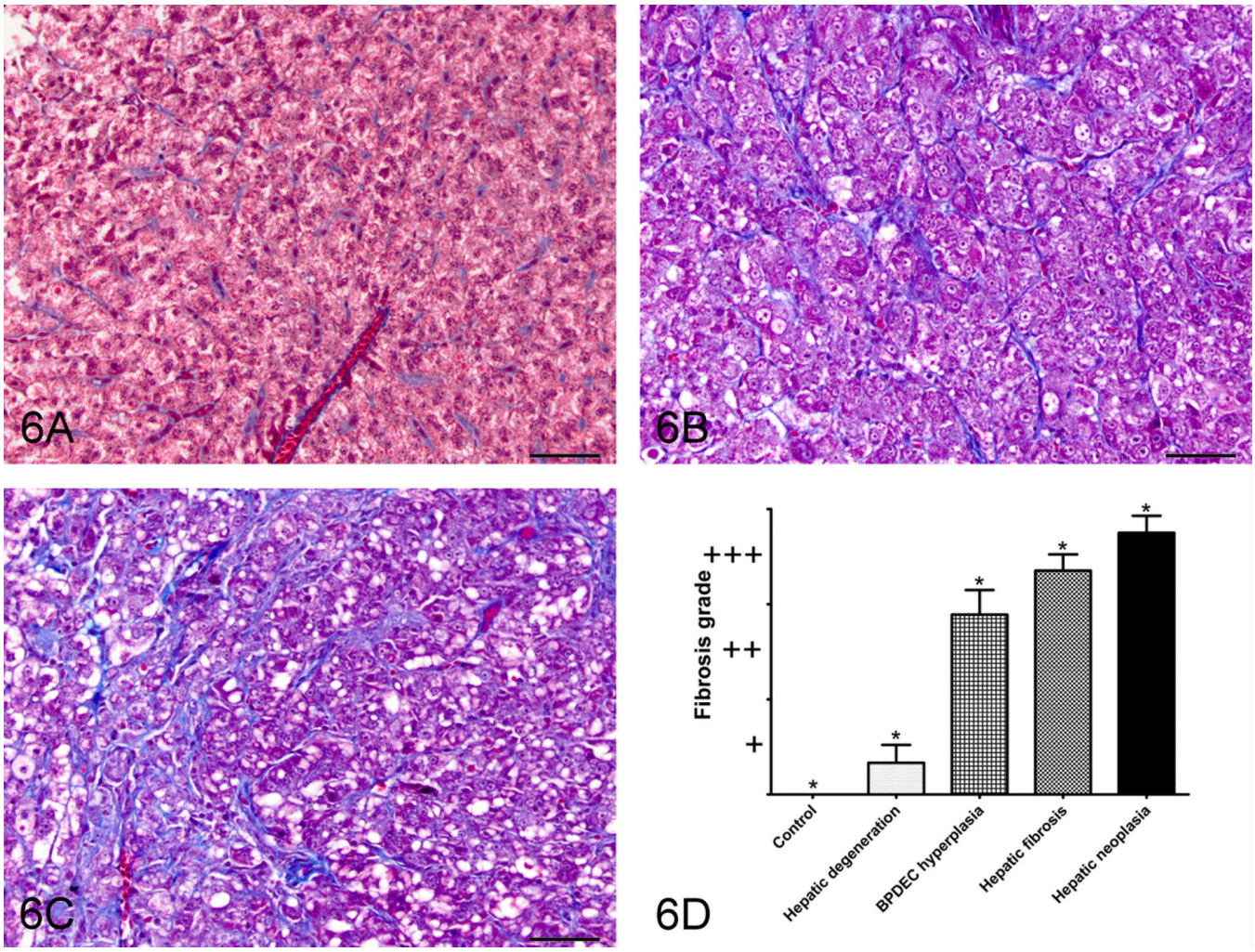

Figure 6.

Masson's trichrome staining as a semi-quantitative measure of collagen deposition. A: Representative picture of control liver; B: grade 2, moderate fibrosis; C: Grade 3, severe fibrosis/cirrhosis. 40X bar = 50um. D: Relationship between phenotype and the fibrosis grade. Semi-quantitative scoring of Masson's trichrome stained slides as a measure of collagen deposition.

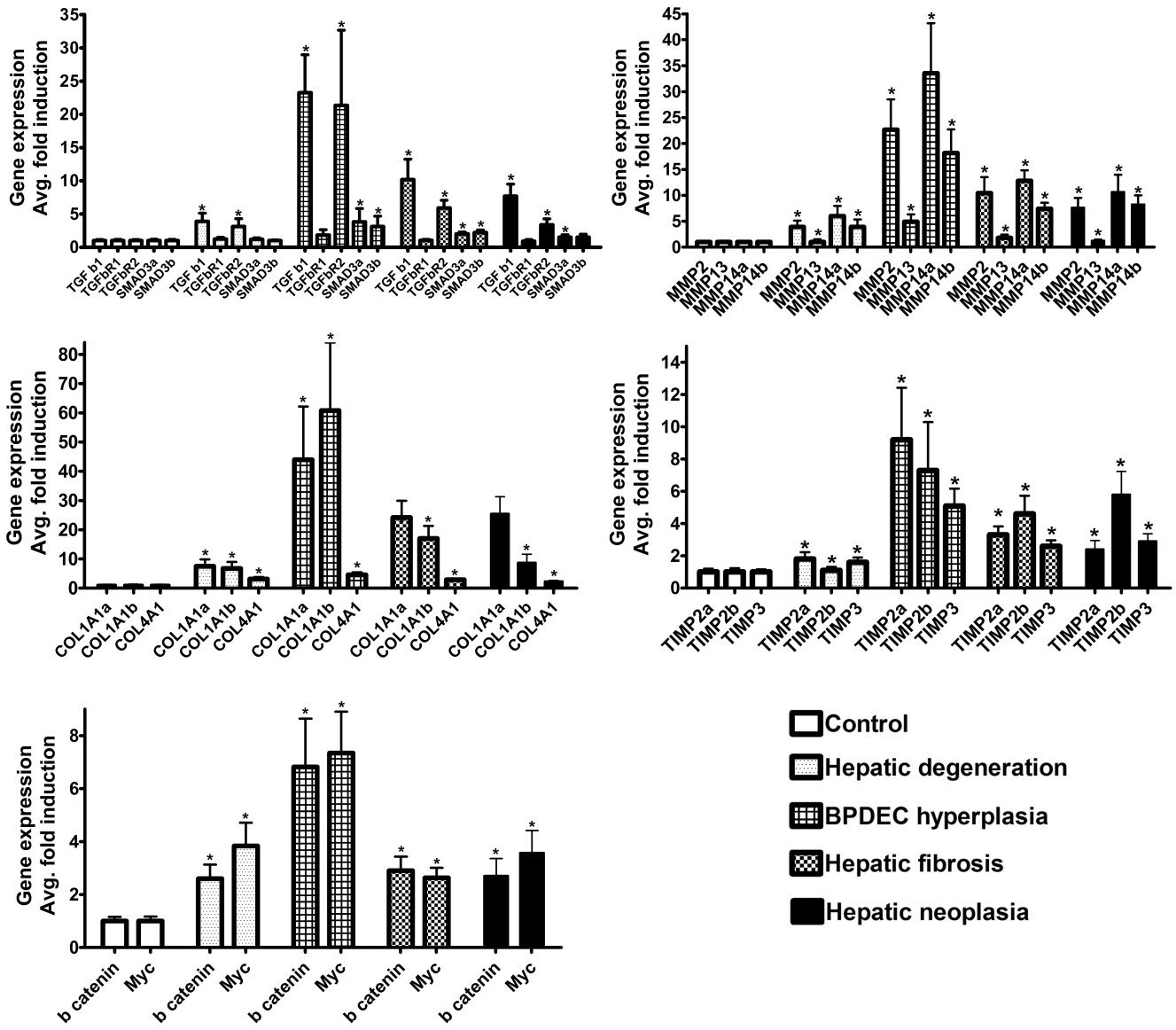

Figure 7.

Relationship between the liver phenotypes observed following DMN exposure and the expression of mammalian fibrosis-related genes. Mean ± SEM. * Statistical difference ($P < 0.05$) in gene expression level between phenotypes.

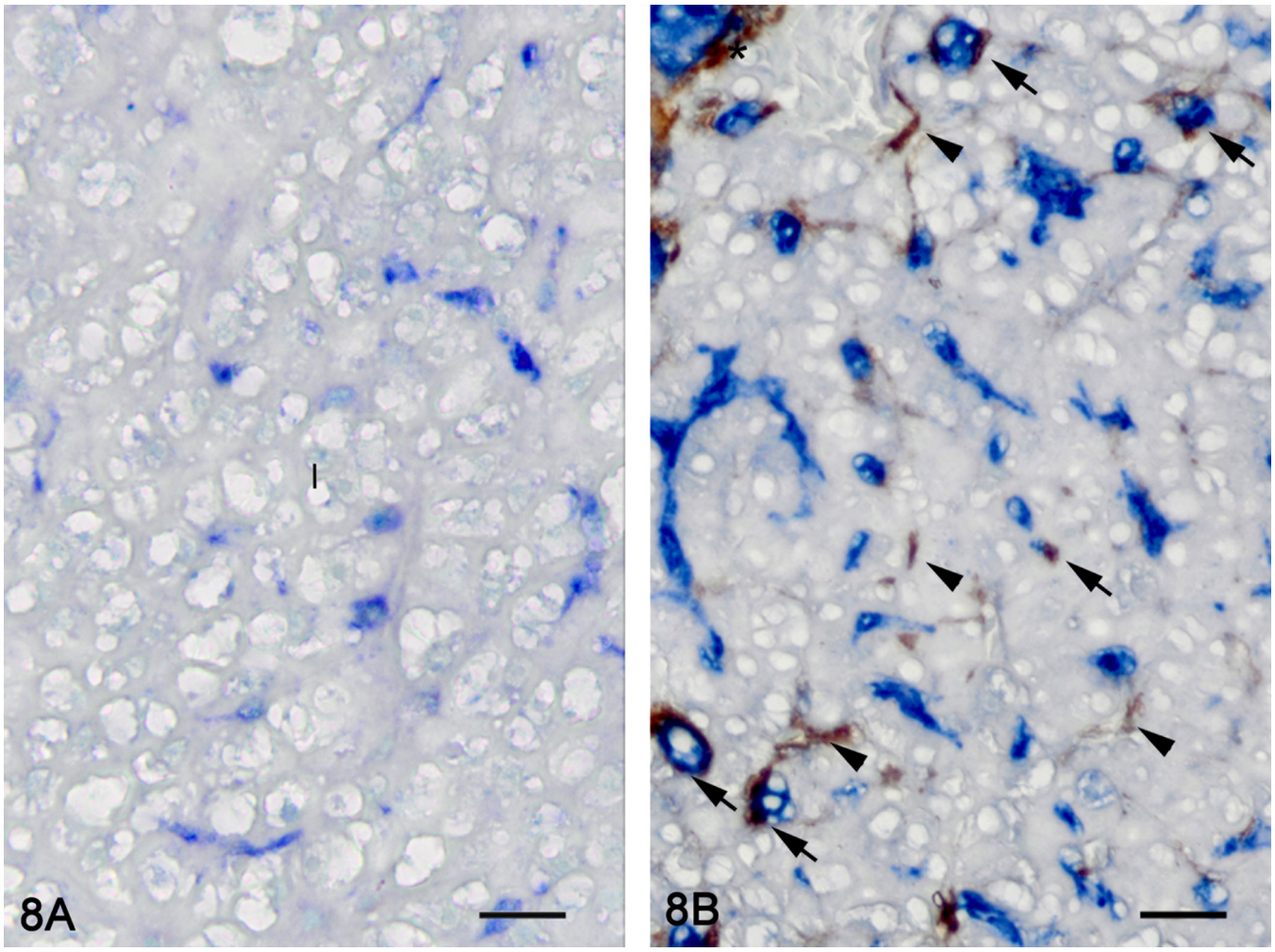

Figure 8.

Hepatic fibrosis. Double immunolabelling for MSA (brown) and TGF-β1 (blue), methyl green counterstain. Representative picture of a control liver (8A). No immunoreactivity for MSA is observed in the hepatic parenchyma. TGF- β1 immunoreactivity is observed in BPDEC. Representative picture of a liver with hepatic fibrosis (8B). BPDEC are increased in number, hypertrophied and strongly positive for TGF- β1. Myofibroblasts (asterisk) and HSCs (arrow head) are immunoreactive for MSA. Some HSCs are immunoreactive for MSA and TGF-β1 (arrow). Bar = 20 μm 100X.

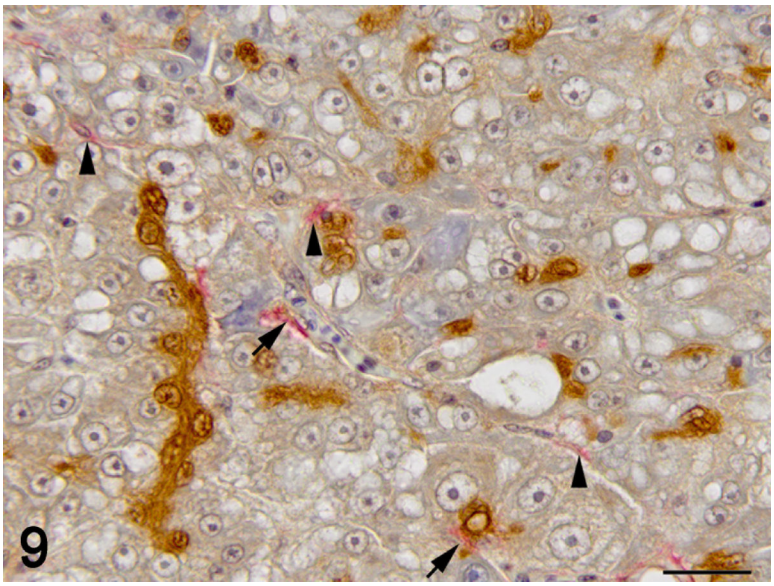

Figure 9.

Hepatic fibrosis. Double immunolabelling for MSA (red) and TGF-β1 (brown), hematoxylin counterstain. BPDEC are increased in number, hypertrophied and strongly positive for TGF-β1. HSCs (arrow head) are immunoreactive for MSA. Some HSCs are immunoreactive for MSA and TGF- β1 (arrow). Bar = 20 μm 100X.

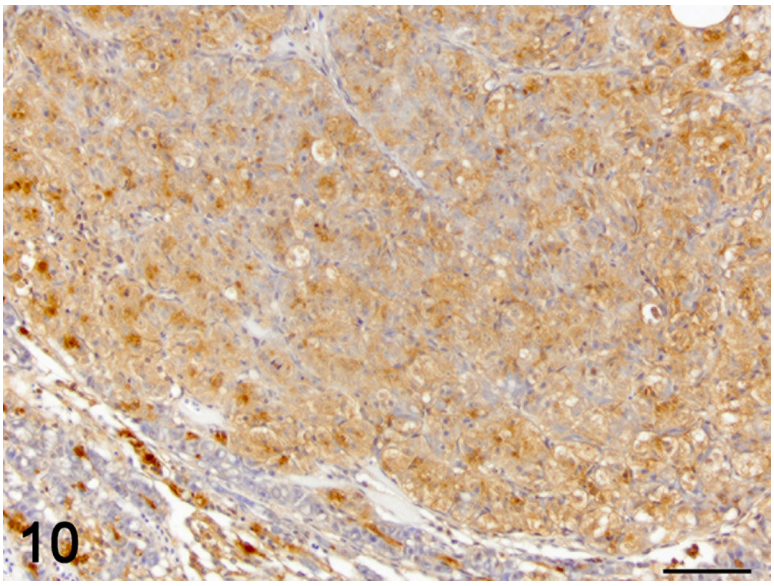

Figure 10.

Hepatocellular carcinoma. Immunolabelling TGF-β1 (brown), hematoxylin counterstain. Most neoplastic hepatocytes display moderate cytoplasmic immunoreactivity for TGF-β1. The BPDECs in the adjacent compressed hepatic parenchyma are strongly positive for TGF-β1 as in control liver. Bar = 50 μm 40X.

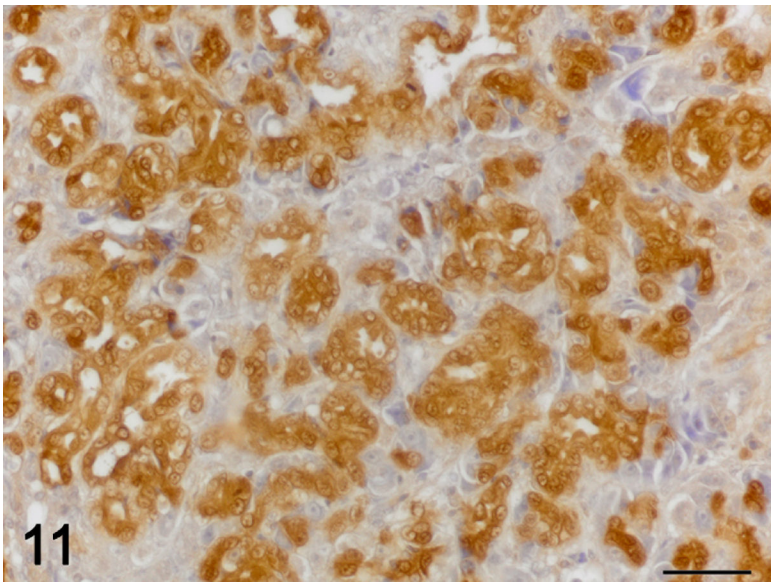

Figure 11.

Cholangiocarcinoma. Immunolabelling for TGF-β1 (brown), hematoxylin counterstain. Neoplastic cholangiocytes display strong cytoplasmic immunoreactivity for TGF-β1. 60X bar = 30um.

Table 1

Sequences for primers used in quantitative, real-time PCR

Primer name	Ensembl gene identifying number*	Sequence (5′→3′)
col1a1a F	ENSORLG00000017013	AAGAAGCACGTCTGGTTTGG
col1a1a R	ENSORLG00000017013	AAACAGACGGGTCCAACTTC
col1a1b F	ENSORLG00000011273	GGTTCTGCTGGTAACGATGG
col1a1b R	ENSORLG00000011273	CCAGGCATTCCAATAAGACC
col4a1 F	ENSORLG00000018010	CCAGGAGATGTTGTCATTGC
col4a1 R	ENSORLG00000018010	CCCTTGATGCCTTCTTTAGC
ctnnb1 F	ENSORLG00000005845	CCACCAGAGCAATACCAGAAC
ctnnb1 R	ENSORLG00000005845	AGCCGTTTCCACATCGTTAG
mmp2 F	ENSORLG00000013688	ACTGAGGGCAGAGATGATGG
mmp2 R	ENSORLG00000013688	TTTCAGGGCAGAAGCCATAG
mmp13 F	ENSORLG00000014453	AACGGCAAGAAGGTGAAGC
mmp13 R	ENSORLG00000014453	CTCAGCTCTGGATCACATCG
mmp14a F	ENSORLG00000007318	CAGGGTCTGAAGTGGGAGAA
mmp14a R	ENSORLG00000007318	ACGGAAGGTGAGTGGGATAA
mmp14b F	ENSORLG00000012159	AGGACAAGACGAAGGAGAAGG
mmp14b R	ENSORLG00000012159	ACAGGAATAACGGCAAGACC
myc F	ENSORLG00000007021	ACAAGCGCATGACTCACAAC
myc R	ENSORLG00000007021	TCTCAGGATCACCACCTTTG
rpl7 F	ENSORLG00000007967	CGCCAGATCTTCAACGGTGTAT
rpl7 R	ENSORLG00000007967	AGGCTCAGCAATCCTCAGCAT
timp2a F	ENSORLG00000010908	AGCAGGCTTGAAAACAGTGC
timp2a R	ENSORLG00000010908	ATCCTCTTGATGGGGTTTCC
timp2b F	ENSORLG00000007689	AGTTCTGACCCCAACATCG
timp2b R	ENSORLG00000007689	GCCGTCCTACCAATTTTGC
timp3 F	ENSORLG00000009218	GCCTTTTGGAACGATACGC
timp3 R	ENSORLG00000009218	ACCTTGCCATCATACACACG
tgfb1 F	ENSORLG00000001272	AAGTGGCTGTCCTTTGACG
tgfb1 R	ENSORLG00000001272	TATCCGCTTCTTCTCCATCC
tgfbr1 F	ENSORLG00000018380	AAAGATAACGGGACGTGGAC
tgfbr1 R	ENSORLG00000018380	ACGTGCCATTCTTCTTCACC
tgfbr2 F	ENSORLG00000014158	GCCAACGTGTGTAAATGGTG
tgfbr2 R	ENSORLG00000014158	ATAACAGGCGAGGGTTGATG
smad3a F	ENSORLG00000002207	GGAAGAAGGGAGAACAGAACG
smad3a R	ENSORLG00000002207	AGACGACCATCCAAAGACC
smad3b F	ENSORLG00000006803	GCTTTGAGGCAGTCTACCAG
smad3b R	ENSORLG00000006803	GGGAATAGACCTCTTCCTAAG

Note: PCR: polymerase chain reaction; col1a1: collagen type I alpha 1; ctnnb1: beta-catenin; mmp: matrix metalloproteinase; timp: tissue inhibitors of metalloproteinase; tgfb1: transforming growth factor beta 1; smad3: mothers against decapentaplegic homolog 3.

* http://www.ensembl.org/index.html

Table 2

Degenerative and Proliferative Hepatic Lesions in Medaka exposed to 100 ppm Dimethylnitrosamine for 2 weeks.

Week post exposure	Cellular degenera-tion	Spongiosis hepatis	Necrosis / apoptosis	Archite-ctural change	BPDEC[a] prolifera-tion	Bile duct hyperplasia	Fibrosis	Cellular dysplasia	Neopl-asia
2 weeks	21/23	3/23	18/23	7/23	6/23	0/23	2/23	5/23	0/23
4 weeks	18/24	15/24	22/24	22/24	21/24	10/24	20/24	18/24	0/24
6 weeks	20/24	18/24	23/24	21/24	19/24	15/24	19/24	17/24	2/24
10 weeks	24/24	19/24	24/24	12/24	23/24	22/24	22/24	22/24	14/24

[a] Bile preductular epithelial cell